

## CASE 2: DETAILS AND SUBMISSION GUIDELINES

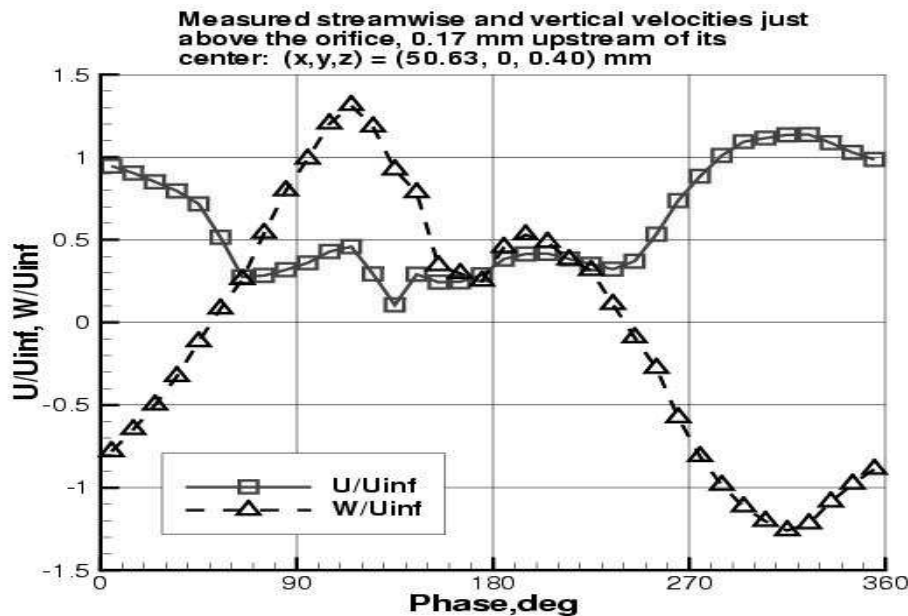
### Relevant Details

The freestream Mach number is  $M_{\text{freestream}} = 0.10$ . The atmospheric conditions varied, but were essentially standard atmospheric conditions at sea level, in a wind tunnel vented to the atmosphere, in a temperature-controlled room. These conditions can be given as approximately:  $p_{\text{ambient}} = \text{approx } 101325 \text{ kg/(m}\cdot\text{s}^2)$   $T_{\text{ambient}} = \text{approx } 75 \text{ deg F (approx } 297 \text{ K)}$ . Some derived relevant conditions are:  $\text{density}_{\text{ambient}} = \text{approx } 1.185 \text{ kg/m}^3$   $\text{viscosity}_{\text{ambient}} = \text{approx } 18.4\text{e-}6 \text{ kg/(m}\cdot\text{s)}$ ,  $u_{\text{freestream}} = \text{approx } 34.6 \text{ m/s}$ , and  $\text{Re}_{\text{freestream}} = \text{approx } 2.23\text{e}6$  per meter.

The upstream boundary conditions from the experiment (associated with the boundary layer on the plate at location  $x=50800$  microns (50.8 mm) upstream of the center of the jet orifice), to be used to help set/verify CFD inflow BCs, are given in the file located on the website.

The diaphragm frequency = 150.0 Hz. The "neutral position" of the moveable diaphragm plate at rest inside the cavity is approximately 2.8 mm below the upper cavity wall (see Geometry page for details). However, when the wind tunnel is on and when the moveable piston is operating, the neutral position of the plate moves up so that it is approximately 1.7 mm below the upper cavity wall. *This change in the neutral position is not accounted for in the current CFD grids available from this website.* However, it is not known whether accounting for this shift is important or not. The plate then displaces sinusoidally about this new neutral position with a maximum displacement of approximately  $\pm 0.77$  mm. The file located on the website lists data from the cavity, including cavity pressure, voltage input, and displacement data about its neutral position.

The pressure is measured inside the cavity on its top wall, to one side of the orifice, approximately on the order of 10 mm from the side wall. The pressure is measured with respect to the tunnel static pressure. The following figure shows the measured phase-averaged streamwise and vertical velocities over the (approximate) center of the orifice as a function of phase.



These LV-derived data over the orifice (plus other quantities of interest) are given in a file located on the website. Note in the data file that the spanwise ( $v$ ) velocity as measured is not near zero.

## Submission Guidelines

Numerical predictions of this type of statistically unsteady flow are relatively new. The purpose here is to determine the state-of-the-art in modeling these types of unsteady synthetic-jet-type flows, so we want to explore which CFD methods work and which do not.

- Either model the internal cavity or specify an unsteady boundary condition at the orifice exit.
- Either model the moving diaphragm, or you may employ an unsteady boundary condition that approximates its effect within the cavity.

There is the requirement that you detail specifically how you choose to model the case, including all boundary conditions and approximations made. As we assess the methodologies used at the workshop, it will be important to know as many details as possible about the calculations/ simulations.

Detailed requirements include:

1. The case must be run time-accurately and in three-dimensions, in order to simulate the unsteady 3-D nature of the case.
  - 1a. RANS codes run in time-accurate mode (e.g., URANS) solve directly for phase-averaged variables, i.e.  $\langle u_i \rangle$  and  $\langle u'_i u'_j \rangle$ . (see Appendix in Case 1: Details and Submission GuidelinesClick). Therefore, RANS simulations should result in repeating or very-nearly-repeating periodic solutions. When periodicity is achieved, averages over one or more periods of oscillation yields the long-time-averaged (time-independent mean) values for these quantities.
  - 1b. DNS, LES, or DES simulations will need to be post-processed to obtain both the phase-averaged and long-time-averaged (time-independent mean) values.
2. GRID STUDY: Solutions using more than one grid size are encouraged, but not required. If you use more than one grid, submit each set of results separately.
3. TIME STEP STUDY: Solutions using more than one time step are encouraged, but not required. If you use more than one time step, submit each set of results separately.

Specific quantities that result from your computations at particular locations will be required for submission. Note that for all the following, we adopt the coordinate system with  $x$  downstream,  $z$  up, and  $y$  spanwise, with the  $(x,y,z)=(0,0,0)$  origin on the tunnel splitter plate 8 diameters (50.8 mm) directly upstream of the center of the orifice (the orifice diameter is 0.25 inches = 6.35 mm). The requirements follow (if it is not possible to provide a particular quantity, simply leave it out of the "variable" list, and reduce the number of columns of data submitted):

a. Long-time-averaged downstream velocity ( $u$ ), spanwise velocity ( $v$ ), and vertical velocity ( $w$ ) profiles (nondimensionalized by  $U_{inf}$ ) along vertical lines at the centerplane ( $y=0$ ) and:  $x=0$  mm,  $x=44.45$  mm (-1D upstream),  $x=50.8$  mm (center of orifice),  $x=57.15$  mm (1D downstream),  $x=63.5$  mm (2D downstream),  $x=76.2$  mm (4D downstream), and  $x=101.6$  mm (8D downstream). Give these data to at least a height of 50 mm. Also, submit horizontal lines of results at  $x=57.15$  mm and:  $z=5$  mm,  $z=10$  mm, and  $z=20$  mm; and also at  $x=63.5$  mm and:  $z=5$  mm,  $z=10$  mm, and  $z=20$  mm. Give these data to at least a width of 25 mm to either side of the orifice. Also, submit horizontal lines of results at  $y=0$ ,  $z=0.4$  mm over the slot (from approx  $x=47.625$  mm to  $x=53.975$  mm), and at  $y=0$ ,  $z=10$  mm from at least  $x=45$  mm to  $x=70$  mm. Name this file: case2.avgvel.ANYTHING.dat-where "ANYTHING" can be any descriptor you choose (should be different for each file if you are submitting multiple runs)-the file should be in 6-column format:

- 1st line: #your name (pound sign needed)
- 2nd line: #your affiliation (pound sign needed)
- 3rd line: #your contact info (pound sign needed)
- 4th line: #brief description of grid (pound sign needed)
- 5th line: #number of time steps per cycle (pound sign needed)
- 6th line: #brief description of code/method (pound sign needed)
- 7th line: #other info about the case, such as spatial accuracy (pound sign needed)

8th line: #other info about the case, such as turb model (pound sign needed)  
 9th line: #other info about the case (pound sign needed)  
 10th line: variables="x, mm", "y, mm", "z, mm", "u/Uinf", "v/Uinf", "w/Uinf"  
 11th line: zone t="data along x=0, y=0"  
 subsequent lines: x(mm) y(mm) z(mm) u/Uinf v/Uinf w/Uinf <- this is the data along x=0, y=0, next line: zone t="data along x=44.45mm, y=0"  
 subsequent lines: x(mm) y(mm) z(mm) u/Uinf v/Uinf w/Uinf <- this is the data along x=44.45, y=0, next line: zone t="data along x=50.8mm, y=0"  
 subsequent lines: x(mm) y(mm) z(mm) u/Uinf v/Uinf w/Uinf <- this is the data along x=50.8, y=0, next line: zone t="data along x=57.15mm, y=0"  
 subsequent lines: x(mm) y(mm) z(mm) u/Uinf v/Uinf w/Uinf <- this is the data along x=57.15, y=0, next line: zone t="data along x=63.5mm, y=0"  
 subsequent lines: x(mm) y(mm) z(mm) u/Uinf v/Uinf w/Uinf <- this is the data along x=63.5, y=0, next line: zone t="data along x=76.2mm, y=0"  
 subsequent lines: x(mm) y(mm) z(mm) u/Uinf v/Uinf w/Uinf <- this is the data along x=76.2, y=0, next line: zone t="data along x=101.6mm, y=0"  
 subsequent lines: x(mm) y(mm) z(mm) u/Uinf v/Uinf w/Uinf <- this is the data along x=101.6, y=0, next line: zone t="data along x=57.15mm, z=5mm"  
 subsequent lines: x(mm) y(mm) z(mm) u/Uinf v/Uinf w/Uinf <- this is the data along x=57.15, z=5, next line: zone t="data along x=57.15mm, z=10mm"  
 subsequent lines: x(mm) y(mm) z(mm) u/Uinf v/Uinf w/Uinf <- this is the data along x=57.15, z=10, next line: zone t="data along x=57.15mm, z=20mm" subsequent lines: x(mm) y(mm) z(mm) u/Uinf v/Uinf w/Uinf <- this is the data along x=57.15, z=20 next line: zone t="data along x=63.5mm, z=5mm"  
 subsequent lines: x(mm) y(mm) z(mm) u/Uinf v/Uinf w/Uinf <- this is the data along x=63.5, z=5, next line: zone t="data along x=63.5mm, z=10mm"  
 subsequent lines: x(mm) y(mm) z(mm) u/Uinf v/Uinf w/Uinf <- this is the data along x=63.5, z=10, next line: zone t="data along x=63.5mm, z=20mm"  
 subsequent lines: x(mm) y(mm) z(mm) u/Uinf v/Uinf w/Uinf <- this is the data along x=63.5, z=20, next line: zone t="data along z=0.4mm, y=0"  
 subsequent lines: x(mm) y(mm) z(mm) u/Uinf v/Uinf w/Uinf <- this is the data along z=0.4, y=0, next line: zone t="data along z=10mm, y=0"  
 subsequent lines: x(mm) y(mm) z(mm) u/Uinf v/Uinf w/Uinf <- this is the data along z=10, y=0

b. Phase-averaged quantities at 9 different phases during the cycle: 0 deg, 40 deg, 80 deg, 120 deg, 160 deg, 200 deg, 240 deg, 280 deg, 320 deg.; where you should align the phases of your computation as described below. Submit the following phase-averaged  $\langle \rangle$  quantities:  $u/Uinf$ ,  $v/Uinf$ ,  $w/Uinf$ ,  $u'u'bar/Uinf^2$ ,  $v'v'bar/Uinf^2$ ,  $w'w'bar/Uinf^2$ ,  $u'v'bar/Uinf^2$ ,  $u'w'bar/Uinf^2$ ,  $v'w'bar/Uinf^2$  (nondimensionalized), where:  $u$  = phase-averaged downstream velocity component,  $v$  = phase-averaged spanwise velocity component,  $w$  = phase-averaged vertical velocity component,  $u'u'bar$  = phase-averaged turbulent normal stress in downstream direction  $v'v'bar$  = phase-averaged turbulent normal stress in spanwise direction,  $w'w'bar$  = phase-averaged turbulent normal stress in vertical direction,  $u'v'bar$  = phase-averaged turbulent shear stress in x-y plane,  $u'w'bar$  = phase-averaged turbulent shear stress in x-z plane,  $v'w'bar$  = phase-averaged turbulent shear stress in y-z plane The locations for these data are the same as for the long-time-averaged quantities. Name these files:

case2.phase000.ANYTHING.dat	case2.phase040.ANYTHING.dat
case2.phase080.ANYTHING.dat	case2.phase120.ANYTHING.dat
case2.phase160.ANYTHING.dat	case2.phase200.ANYTHING.dat
case2.phase240.ANYTHING.dat	case2.phase280.ANYTHING.dat
case2.phase320.ANYTHING.dat	

-where "ANYTHING" can be any descriptor you choose (should be different for each file if you are submitting multiple runs)-the file should be in 12-column format:

1st line: #your name (pound sign needed)  
 2nd line: #your affiliation (pound sign needed)

3rd line: #your contact info (pound sign needed)  
 4th line: #brief description of grid (pound sign needed)  
 5th line: #number of time steps per cycle (pound sign needed)  
 6th line: #brief description of code/method (pound sign needed)  
 7th line: #other info about the case, such as spatial accuracy (pound sign needed)  
 8th line: #other info about the case, such as turb model (pound sign needed)  
 9th line: #other info about the case (pound sign needed)  
 10th line variables="x, mm";"y, mm"; "z, mm", "u/Uinf", "v/Uinf", "w/Uinf",  
 "uu/Uinf", "vv/Uinf", "ww/Uinf", "uv/Uinf", "uw/Uinf", "vw/Uinf",  
 11th line: zone t="data along x=0, y=0"  
 subsequent lines: x(mm) y(mm) z(mm) u/Uinf v/Uinf w/Uinf uu/Uinf^2 vv/Uinf^2  
 ww/Uinf^2 uv/Uinf^2 uw/Uinf^2 vw/Uinf^2 <- this is the data along x=0, y=0  
 next line: zone t="data along x=44.45mm, y=0"  
 subsequent lines: x(mm) y(mm) z(mm) u/Uinf v/Uinf w/Uinf uu/Uinf^2 vv/Uinf^2  
 ww/Uinf^2 uv/Uinf^2 uw/Uinf^2 vw/Uinf^2 <- this is the data along x=44.45, y=0  
 next line: zone t="data along x=50.8mm, y=0"  
 subsequent lines: x(mm) y(mm) z(mm) u/Uinf v/Uinf w/Uinf uu/Uinf^2 vv/Uinf^2  
 ww/Uinf^2 uv/Uinf^2 uw/Uinf^2 vw/Uinf^2 <- this is the data along x=50.8, y=0  
 next line: zone t="data along x=57.15mm, y=0"  
 subsequent lines: x(mm) y(mm) z(mm) u/Uinf v/Uinf w/Uinf uu/Uinf^2 vv/Uinf^2  
 ww/Uinf^2 uv/Uinf^2 uw/Uinf^2 vw/Uinf^2 <- this is the data along x=57.15, y=0  
 next line: zone t="data along x=63.5mm, y=0"  
 subsequent lines: x(mm) y(mm) z(mm) u/Uinf v/Uinf w/Uinf uu/Uinf^2 vv/Uinf^2  
 ww/Uinf^2 uv/Uinf^2 uw/Uinf^2 vw/Uinf^2 <- this is the data along x=63.5, y=0  
 next line: zone t="data along x=76.2mm, y=0"  
 subsequent lines: x(mm) y(mm) z(mm) u/Uinf v/Uinf w/Uinf uu/Uinf^2 vv/Uinf^2  
 ww/Uinf^2 uv/Uinf^2 uw/Uinf^2 vw/Uinf^2 <- this is the data along x=76.2, y=0  
 next line: zone t="data along x=101.6mm, y=0"  
 subsequent lines: x(mm) y(mm) z(mm) u/Uinf v/Uinf w/Uinf uu/Uinf^2 vv/Uinf^2  
 ww/Uinf^2 uv/Uinf^2 uw/Uinf^2 vw/Uinf^2 <- this is the data along x=101.6, y=0  
 next line: zone t="data along x=57.15mm, z=5mm"  
 subsequent lines: x(mm) y(mm) z(mm) u/Uinf v/Uinf w/Uinf uu/Uinf^2 vv/Uinf^2  
 ww/Uinf^2 uv/Uinf^2 uw/Uinf^2 vw/Uinf^2 <- this is the data along x=57.15, z=5  
 next line: zone t="data along x=57.15mm, z=10mm"  
 subsequent lines: x(mm) y(mm) z(mm) u/Uinf v/Uinf w/Uinf uu/Uinf^2 vv/Uinf^2  
 ww/Uinf^2 uv/Uinf^2 uw/Uinf^2 vw/Uinf^2 <- this is the data along x=57.15, z=10  
 next line: zone t="data along x=57.15mm, z=20mm"  
 subsequent lines: x(mm) y(mm) z(mm) u/Uinf v/Uinf w/Uinf uu/Uinf^2 vv/Uinf^2  
 ww/Uinf^2 uv/Uinf^2 uw/Uinf^2 vw/Uinf^2 <- this is the data along x=57.15, z=20  
 next line: zone t="data along x=63.5mm, z=5mm"  
 subsequent lines: x(mm) y(mm) z(mm) u/Uinf v/Uinf w/Uinf uu/Uinf^2 vv/Uinf^2  
 ww/Uinf^2 uv/Uinf^2 uw/Uinf^2 vw/Uinf^2 <- this is the data along x=63.5, z=5  
 next line: zone t="data along x=63.5mm, z=10mm"  
 subsequent lines: x(mm) y(mm) z(mm) u/Uinf v/Uinf w/Uinf uu/Uinf^2 vv/Uinf^2  
 ww/Uinf^2 uv/Uinf^2 uw/Uinf^2 vw/Uinf^2 <- this is the data along x=63.5, z=10  
 next line: zone t="data along x=63.5mm, z=20mm"  
 subsequent lines: x(mm) y(mm) z(mm) u/Uinf v/Uinf w/Uinf uu/Uinf^2 vv/Uinf^2  
 ww/Uinf^2 uv/Uinf^2 uw/Uinf^2 vw/Uinf^2 <- this is the data along x=63.5, z=20  
 next line: zone t="data along z=0.4mm, y=0"  
 subsequent lines: x(mm) y(mm) z(mm) u/Uinf v/Uinf w/Uinf uu/Uinf^2 vv/Uinf^2  
 ww/Uinf^2 uv/Uinf^2 uw/Uinf^2 vw/Uinf^2 <- this is the data along z=0.4, y=0  
 next line: zone t="data along z=10mm, y=0"  
 subsequent lines: x(mm) y(mm) z(mm) u/Uinf v/Uinf w/Uinf uu/Uinf^2 vv/Uinf^2  
 ww/Uinf^2 uv/Uinf^2 uw/Uinf^2 vw/Uinf^2 <- this is the data along z=10, y=0

The sample datafile case2.phase000.SAMPLE.dat can be downloaded from the website

c. Phase-averaged time-history values of  $\langle u \rangle$ ,  $\langle v \rangle$ , and  $\langle w \rangle$  (nondimensionalized by  $U_{inf}$ ) as a function of phase (deg) at three approximate point locations:  $(x,y,z)=(50.63, 0, 0.40)$ mm,  $(57.15, 0, 10)$ mm, and  $(63.5, 0, 10)$ mm. Give the data at every time step taken. In other words, if the time step yields 100 steps per cycle, then give 100 phases between 0 deg and 360 deg. The phases of your computation should be aligned as described below. Name this file: case2.phasehist.ANYTHING.dat-where "ANYTHING" can be any descriptor you choose (should be different for each file if you are submitting multiple runs)-the file should be in 7-column format:

1st line: #your name (pound sign needed)  
2nd line: #your affiliation (pound sign needed)  
3rd line: #your contact info (pound sign needed)  
4th line: #brief description of grid (pound sign needed)  
5th line: #number of time steps per cycle (pound sign needed)  
6th line: #brief description of code/method (pound sign needed)  
7th line: #other info about the case, such as spatial accuracy (pound sign needed)  
8th line: #other info about the case, such as turb model (pound sign needed)  
9th line: #other info about the case (pound sign needed)  
10th line: variables="phase, deg","x, mm","y, mm","z, mm","u/Uinf","v/Uinf","w/Uinf"  
11th line: zone t="x=50.63mm, y=0mm, z=0.4mm"  
subsequent lines: phase x(mm) y(mm) z(mm) u/Uinf v/Uinf w/Uinf <- this is the data at x=50.63, y=0, z=0.4  
next line: zone t="x=57.15mm, y=0mm, z=10mm"  
subsequent lines: phase x(mm) y(mm) z(mm) u/Uinf v/Uinf w/Uinf <- this is the data at x=57.15, y=0, z=10  
next line: zone t="x=63.5mm, y=0mm, z=10mm"  
subsequent lines: phase x(mm) y(mm) z(mm) u/Uinf v/Uinf w/Uinf <- this is the data at x=63.5, y=0, z=10

The sample datafile case2.phasehist.SAMPLE.dat should be downloaded from the website

d. Field line-contour-plots (in one of the following formats: ps, eps, or jpg) of long-time-averaged streamwise velocity ( $u/U_{inf}$ ) in the planes  $y=0$ mm (centerplane),  $x=57.15$ mm (1D downstream), and  $x=76.2$ mm (4D downstream). These plots should be black-and-white line plots. The  $y=0$  plane plot should go from approx  $x=45$ mm to 125mm and  $z=0$  to 36mm. The  $x=const$ -plane plots should go from approx  $y=-18$ mm to +18mm, and  $z=0$  to 36mm. The  $x$ -to- $z$  ratio of the plots should be 1.0. Plot  $u/U_{inf}$  line contours of -0.5 through 1.5 in increments of 0.1. Label the contour lines, if possible. The purpose of submitting these plots is to get a qualitative picture of the long-time-averaged flowfield, indicative of the dynamic range of the orifice's influence. Altogether, submit 3 plot files. Name these files: case2.uavg.y0.ANYTHING.eps case2.uavg.x57.15.ANYTHING.eps case2.uavg.x76.2.ANYTHING.eps (where the "eps" in this case means encapsulated postscript - use ps, or jpg instead if appropriate).

e. Field line-contour-plots (in one of the following formats: ps, eps, or jpg) of phase-averaged streamwise velocity ( $\langle u \rangle/U_{inf}$ ) in the planes  $y=0$ mm (centerplane),  $x=57.15$ mm (1D downstream), and  $x=76.2$ mm (4D downstream) at the following phases: 40 deg, 120 deg, 200 deg, and 280 deg.; where you should align the phases of your computation as described below. These plots should be black-and-white line plots. The  $y=0$  plane plots should go from approx  $x=45$ mm to 125mm and  $z=0$  to 36mm. The  $x=const$ -plane plots should go from approx  $y=-18$ mm to +18mm, and  $z=0$  to 36mm. The  $x$ -to- $z$  or  $x$ -to- $y$  ratio of the plot should be 1.0. For all plot files, plot  $\langle u \rangle/U_{inf}$  line contours of -1.0 through 2.0 in increments of 0.1. Either (a) plot the lines of negative velocity as dashed lines and the lines of positive velocity as solid lines, or (b) label the contour lines, or (c) do both. The purpose of submitting these plots is to get a qualitative picture of the phase-averaged flowfield at particular selected times of interest. Altogether, submit 12 plots files. Name these files: case2.phase040.y0.ANYTHING.eps case2.phase120.y0.ANYTHING.eps case2.phase200.y0.ANYTHING.eps

case2.phase280.y0.ANYTHING.eps  
 case2.phase120.x57.15.ANYTHING.eps  
 case2.phase280.x57.15.ANYTHING.eps  
 case2.phase120.x76.2.ANYTHING.eps  
 case2.phase280.x76.2.ANYTHING.eps (where the "eps" in this case means encapsulated postscript - use ps, or jpg instead if appropriate)

case2.phase040.x57.15.ANYTHING.eps  
 case2.phase200.x57.15.ANYTHING.eps  
 case2.phase040.x76.2.ANYTHING.eps  
 case2.phase200.x76.2.ANYTHING.eps

## Definition of Phase for the Computations

Matching the same phases with the experiment is not necessarily straightforward. One way to do it is to try to align a quantity from experiment (such as vertical velocity near the jet exit), but this can be imprecise because the CFD and experimental data are not necessarily well-behaved sine-waves. The best criteria for determining phase may in fact be a different measure altogether.

On the other hand, in this workshop we want to be able to compare CFD results with each other, so it is important to try to achieve the same phase definitions in order that all computations are similarly aligned. We have tried to choose criteria for determining phase that approximates experiment AND is specific enough so that different CFD solutions can be meaningfully compared.

Therefore, although participants are given some latitude to determine phase as appropriate, we encourage everyone to use the following steps to define phase in a uniform fashion for Case 2:

- **Step 1.** Output vertical phase-averaged velocity ( $w$ ) at the following point in space (over the orifice) as a function of your iteration or time step number:  $(x,y,z)=(50.63, 0, 0.40)$ mm. Find  $w_{max}$  and  $w_{min}$  over the course of one phase-averaged period.

- **Step 2.** Compute the mid-value  $w_{avg}=(w_{max}+w_{min})/2$

- **Step 3.** Define Phase=50 deg as the time when your velocity at this location approximately equals  $w_{avg}$  (INCREASING). All other phases can be referenced from this, via the following relation:

$$\text{Phase}=(\text{iter}-\text{it}50)*360/\text{nstep}+50$$

where:

iter =iteration (or time step) number

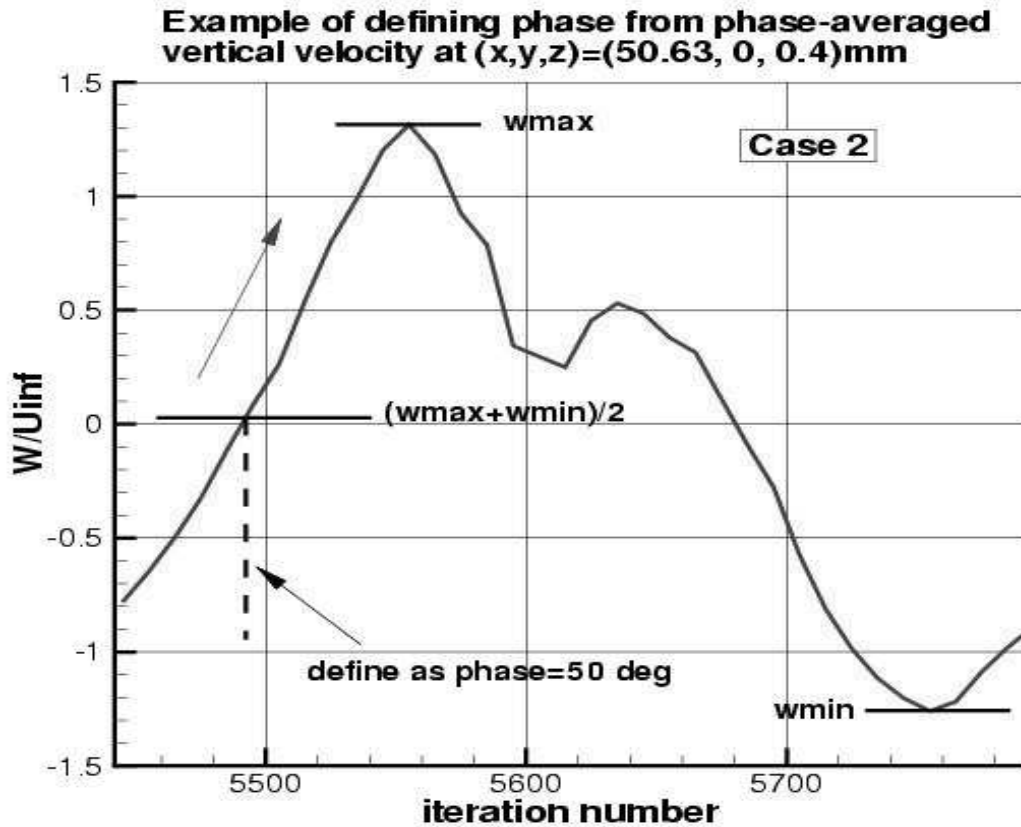
nstep=no. of time steps per cycle

it50=iteration number when Phase=50 according to the above criteria

For example, if you are running 360 steps per cycle and you match the above criteria at time step number 5492, then

$$\text{Phase}=\text{iter}-5442$$

Thus, when iter=5442, then Phase=0; when iter=5622, then Phase=180; when iter=5802, then Phase=360. Note that Phase=360 also corresponds with Phase=0 (it repeats every 360 deg). This is illustrated in the following figure (updated on 24 December 2003):



As another example, say the computation ran 1080 steps per cycle and you match the above criteria at time step number 10002, then

$$\text{Phase} = (\text{iter} - 10002) / 3 + 50$$

Thus, when iter=9852, then Phase=0; when iter=10392, then Phase=180; when iter=10932, then Phase=360.



# CASE 2: SYNTHETIC JET IN A CROSSFLOW

Julien Dandois <sup>†</sup>, Eric Garnier <sup>‡</sup> and Pierre Sagaut <sup>§</sup>

ONERA, BP 72, 29 av. de la division Leclerc, 92322 Châtillon Cedex, France

## 1 Introduction

Three-dimensional, compressible simulations of the interaction between a synthetic jet and a turbulent boundary layer have been performed using Large Eddy Simulation. A modeled boundary condition has been used for the actuator. A study of the effects of the time step, number of sub-iterations in the time integration process, actuator boundary condition has been investigated.

## 2 Solution Methodology

The unsteady, three-dimensional, compressible Navier-Stokes equations are solved using Large-Eddy Simulations. Any flow variable  $\Phi$  can be written as  $\Phi = \bar{\Phi} + \Phi'$ , where  $\bar{\Phi}$  represents the resolved part of the variable and  $\Phi'$  its subgrid part. The filtering operator is classically defined as a convolution product on the grid cell. The FLU3M solver, developed by ONERA, is based on a cell centered finite volume technique and structured multiblock meshes. For efficiency, an implicit time integration is employed to deal with the very small grid size encountered near the wall. The time integration is carried out by means of the backward scheme of Gear which is second-order-accurate:

$$\frac{\partial w}{\partial t} = \frac{\frac{3}{2}w^{n+1} - 2w^n + \frac{1}{2}w^{n-1}}{\delta t} \quad (1)$$

Because of the implicit terms, a non-linear system has to be solved. The Newton-Raphson method is used to compute  $w^{n+1}$ . At each iteration of this inner process, the inversion of the linear system relies on lower-upper symmetric Gauss-Seidel implicit method. More details about these numerical points are available in Ref. [3]. A special effort has been carried out to minimize the intrinsic dissipation of the scheme and the computational cost. The spatial scheme is the scheme proposed by Mary and Sagaut [2]. It is based on the AUSM+(P) [4] scheme, whose dissipation is proportional to the local fluid velocity so it is well adapted to low-Mach number boundary-layer simulations. As we are not interested by the shock capturing properties of the scheme, simplified formulas have been developed to approximate the Euler fluxes:

$$F_1^{i+\frac{1}{2}} = U_1(Q_L + Q_R)/2 - |U_{dis}|(Q_R - Q_L)/2 + P \quad (2)$$

where  $U_1$  denotes the interface fluid velocity,  $L/R$  the left and right third-order MUSCL interpolation. The state vector  $Q$  is defined as  $(\bar{\rho}, \bar{\rho}\bar{u}_1, \bar{\rho}\bar{u}_2, \bar{\rho}\bar{u}_3, \rho E + \bar{p})^t$ , whereas the pressure term  $P$  is given by  $[0, (\bar{p}_L + \bar{p}_R)/2, 0, 0, 0]$ . The symbol  $u_{dis}$ , which indicates a local fluid velocity, characterizes the numerical dissipation acting on the velocity components. It is defined as follows:

$$U_{dis} = \max(|\bar{u}_{1L} + \bar{u}_{1R}|/2, c_1) \quad (3)$$

---

<sup>†</sup>PhD student, ONERA, Applied Aerodynamic Department

<sup>‡</sup>Research Engineer, ONERA, Applied Aerodynamic Department

<sup>§</sup>Professor, Laboratoire de Modélisation pour la Mécanique and ONERA, CFD and Aeroacoustics Department

where  $c_1$  is a constant parameter. To enforce the pressure/velocity coupling in low-Mach-number zone, a pressure stabilization term is added to the interface fluid velocity:

$$U_1 = (u_{1L} + u_{1R})/2 - c_2(\bar{p}_R - \bar{p}_L) \quad (4)$$

where  $c_2$  is a constant parameter. For an accuracy reason the values of  $c_1$  and  $c_2$  should be chosen as small as possible to minimize the numerical dissipation. For a stability reason these parameters cannot be smaller than 0.04. For the viscous fluxes, a second-order-accurate centered scheme is used.

### 3 Model Description

The subgrid scale model used is the selective mixed scales model [1]. This model has been shown to be effective in turbulent flows. The expression of the subgrid viscosity is:

$$\nu_{sm} = C_m(\alpha)|\tilde{S}(\vec{x}, t)|^\alpha \left[ q_c^2(\vec{x}, t) \right]^{\frac{1-\alpha}{2}} \Delta^{1+\alpha} f_s \quad (5)$$

where  $C_m = 0.6$ ,  $\alpha = 0.5$ ,  $f_s$  is a selection function which tests the tridimensionality of the flow (see [1] for more details) and  $q_c$  is the kinetic energy of the smallest resolved scales which is evaluated with a test filter with a cutoff  $\check{\Delta} = \sqrt{6}\Delta$  where  $\Delta$  is the cubic root of the cell volume:

$$q_c^2(\vec{x}, t) = \frac{1}{2}(\tilde{u} - \check{u})(\tilde{u} - \check{u}) \quad \text{where} \quad \check{u}_i = \frac{\tilde{u}_{i-1} + 2\tilde{u}_i + \tilde{u}_{i+1}}{4} \quad (6)$$

### 4 Implementation and Case Specific Details

Table 1 provides the mesh size and grid spacings in the central refined zone of the inflow domain.

Table 1: Computational mesh parameters

$\Delta x$ (mm)	$\Delta y$ (mm)	$\Delta z_{min}$ (mm)	$\Delta x^+$	$\Delta y^+$	$\Delta z^+$
1.16	0.44	0.036	100	36	3

The size of the computational domain is the same than the one of the RANS grid posted on the workshop website: the streamwise length is 152.4mm or 24D (8D upstream and 16D downstream), the spanwise and vertical length are 76mm or approximately 12D. There are 180 points on the jet circumference. The grid is composed of 14 domains. The cells number repartition is shown in Table 2.

Table 2: Cells repartition

External field	Orifice	Cavity	Total
1.25 million	263 000	98 000	1.7 million

Figures 1 and 2 provide a view of the grid in the x-y and x-z planes.

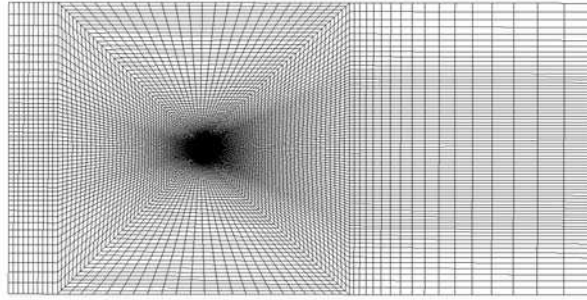


Figure 1: X-Y view of the grid.

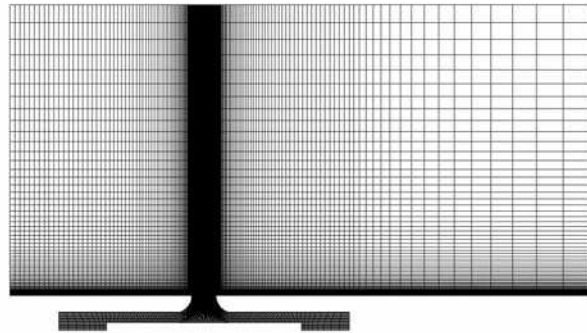


Figure 2: X-Z view of the grid.

The boundary conditions are shown in Fig. 3. On the whole cavity's bottom surface, a blowing/suction condition with a top-hat distribution which varies sinusoidally in time is implemented in order to simulate the diaphragm movement:  $u(x, t) = U_0 * \cos(2\pi ft)$  with  $U_0 = 0.273 m.s^{-1}$  and  $f = 150 Hz$ .  $U_0$  has been calculated using, on the one hand, the sections ratio between the orifice and the cavity bottom surface and, on the other hand, a target output velocity of  $50 m.s^{-1}$ .

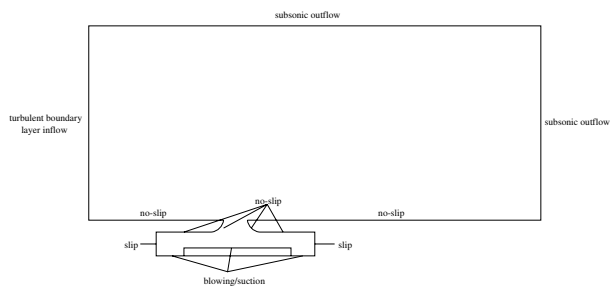


Figure 3: Boundary conditions.

A study of the influence of the actuator boundary condition, time step and number of sub-iterations has been performed. For those case, the blowing/suction condition is applied both on piston and diaphragm. For the case D, instead of using a sinusoidal function, a polynomial fit of driver displacement derivative given on the workshop's website has been used. In that case, the blowing/suction condition is applied only on the piston. The inflow boundary condition is based on a steady RANS mean velocity profile. Realistic turbulent inflow conditions will be implemented in a follow-up of this study. The table 3 shows the different varying parameters.

Table 3: Computational parameters of the study

Case designation	Time step	Number of subiterations	Surface of the boundary condition	$U_0 (m.s^{-1})$
A	$1 \mu s$	4	piston+diaphragm	0.273
B	$1 \mu s$	6	piston+diaphragm	0.273
C	$0.5 \mu s$	4	piston+diaphragm	0.273
D	$1 \mu s$	4	piston	0.725

The figure 4 shows that the solution is not very sensitive to the investigated parameters. For the submitted data, the time step was fixed to  $1 \mu s$  and the number of sub-iterations has been increased to 8 because residues, not shown here, were not sufficiently converged with 6 sub-iterations. On the plot of figures 4 and 5, the phase duration is 10 deg like in the experimental results provided in the website.

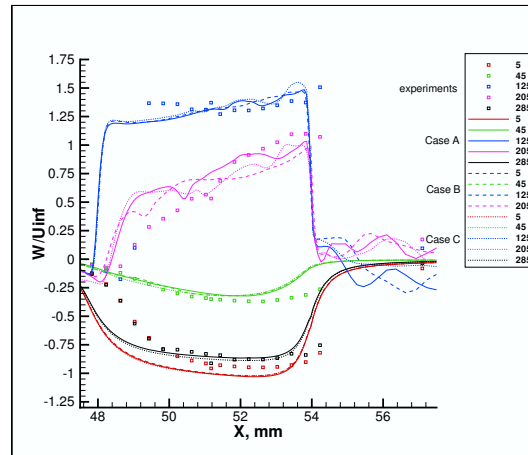


Figure 4: Influence of the time step and the number of sub-iterations on the phase averaged values of  $W/U_{inf}$  after 2 periods at ( $y=0, z=0.4mm$ ).

Although the actuator boundary condition of the case D is more realistic, the results are less accurate than those of the case A (see fig. 5) and the simpler boundary conditions has been finally selected.

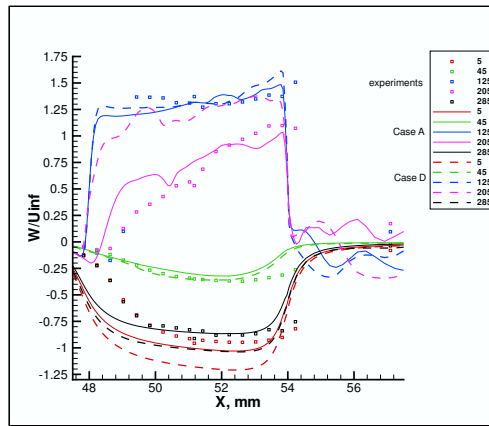


Figure 5: Influence of the actuator boundary condition on the phase averaged values of  $W/U_{inf}$  after 2 periods at ( $y=0, z=0.4\text{mm}$ ).

For the definition of phase, the output vertical velocity has been plotted as a function of time (see fig. 6). The definition given on the workshop website has been used. The submitted data have been phase-averaged on 8 periods.

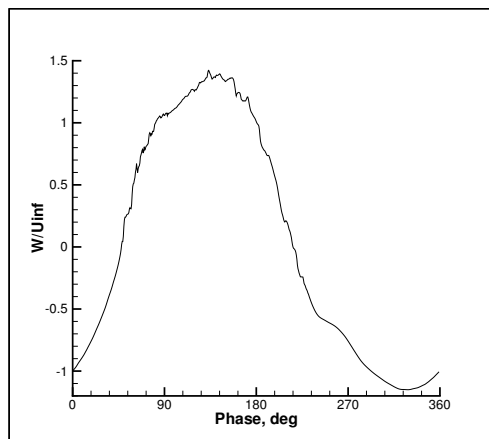


Figure 6: Vertical velocity just above the orifice upstream of the center  $(x,y,z)=(50.63,0,0.4)\text{mm}$ .

## References

- [1] E. Lenormand and P. Sagaut and L. Ta Phuoc and P. Comte “Subgrid-scale models for Large-Eddy Simulation of compressible wall bounded flows”, *AIAA J.*, Vol. 38, No. 8, pp. 1340-1350, 2000.
- [2] I. Mary and P. Sagaut “LES of a flow around an airfoil near stall”, *AIAA J.*, Vol. 40, No. 6, pp. 1139-1145, 2002.
- [3] M. Péchier, P. Guillen and R. Gayzac “Magnus Effectover Finned Projectiles”, *Journal of Spacecrafts and Rockets*, Vol. 38, No. 4, 2001, pp. 542-549.
- [4] J.R. Edwards, M.S. Liou “Low-Diffusion Flux-Splitting Methods for Flows at All Speeds”, *AIAA Journal*, Vol. 36, No. 9, pp. 1610-1617, 1998.



## CASE 2: URANS APPLICATION WITH CFL3D

C. L. Rumsey

*Computational Modeling & Simulation Branch, NASA Langley Research Center, Hampton, VA 23681-2199*

### Solution Methodology

This case was run using CFL3D, a multi-zone Reynolds-averaged Navier-Stokes code developed at NASA Langley [1]. It solves the thin-layer form of the Navier-Stokes equations in each of the (selected) coordinate directions. It can use 1-to-1, patched, or overset grids, and employs local time step scaling, grid sequencing, and multigrid to accelerate convergence to steady state. In time-accurate mode, CFL3D has the option to employ dual-time stepping with subiterations and multigrid, and it achieves second order temporal accuracy.

CFL3D is a finite volume method. It uses third-order upwind-biased spatial differencing on the convective and pressure terms, and second-order differencing on the viscous terms; it is globally second-order spatially accurate. The flux difference-splitting (FDS) method of Roe is employed to obtain fluxes at the cell faces. It is advanced in time with an implicit three-factor approximate factorization method.

### Model Description

For this test case, two different turbulence models have been run to date. The first is the one-equation Spalart-Allmaras model (SA) [2], and the second is the two-equation shear-stress transport model of Menter (SST) [3, 4]. These are both linear eddy-viscosity models that make use of the Boussinesq eddy-viscosity hypothesis. The equations describing these two models can be found in their respective references.

In CFL3D, the models are implemented uncoupled from the mean-flow equations. They are solved using a three-factor implicit approximate factorization approach. The advection terms are discretized with first-order upwind differencing. The production source term is solved explicitly, while the advection, destruction, and diffusion terms are treated implicitly.

### Implementation and Case Specific Details

In this flow, a synthetic jet issues into a turbulent boundary layer through a circular orifice of diameter 6.35 mm in the floor. The flow is characterized by a forcing frequency of 150 Hz, with a maximum discharge vertical velocity of approximately  $1.25U_\infty$ . The approach boundary layer thickness is somewhat greater than 20 mm, the freestream Mach number is  $M = 0.1$ , and the Reynolds number is approximately  $Re = 14160$  per orifice diameter.

The grid used was the supplied structured grid number 1 (which contains 7-zones connected in a 1-to-1 fashion, and approximately 4.09 million grid points), as well as a medium-level grid made from the fine grid by extracting every-other point in each coordinate direction. The SA model was solved on both the fine and medium grids, whereas the SST model was only solved on the medium grid.

The time step chosen was one that yielded 720 time steps per cycle of the forcing frequency. For the SA model, 5 subiterations were employed per time step. For the SST model, however, a large instability was noted when 5 subiterations were employed. This instability showed up as a series of un-physical oscillations in the flowfield variables at given points in space during part of the cycle. By increasing the number of subiterations to 10, the level of this instability decreased, but it did not go away. See for example, Fig. 1, which shows the vertical (W) velocity component as a function of phase 1D downstream of the center of the

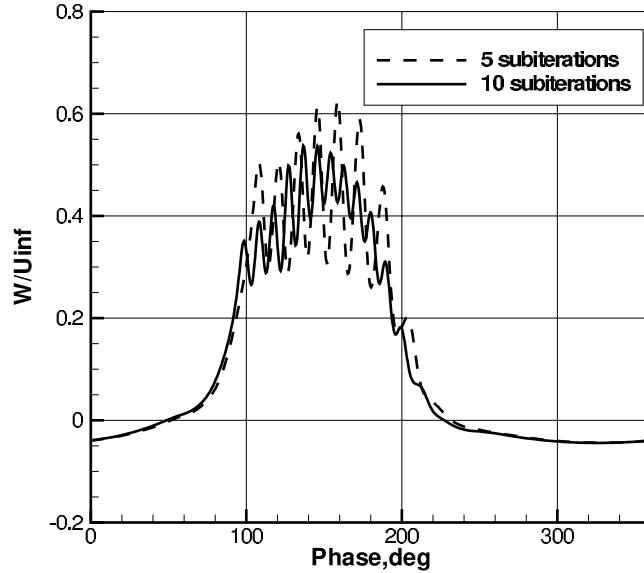


Figure 1: Effect of subiterations on result using SST at  $x=57.15$  mm,  $z=10$  mm (1D downstream), medium grid.

orifice, at  $z=10$  mm above the floor. Therefore, the current SST results should be considered as incomplete; future work will address eliminating the instability.

The boundary conditions were as follows. At the tunnel floor as well as on the inner lip of the orifice and upper wall of the cavity, solid wall adiabatic boundary conditions were applied. The side walls of the cavity were modeled as slip walls, and the bottom surfaces of the cavity employed a time-dependent boundary condition. In other words, the moving diaphragm was modeled on the stationary grid through the use of a boundary condition that imposed a vertical velocity in a sinusoidal manner. (Note that the bottom of the cavity in the supplied grid modeled both the elastic diaphragm as well as the solid plate glued to its center. The time-dependent boundary condition was applied both on the part modeling the elastic diaphragm as well as on the part modeling the solid plate.) The time-dependent boundary condition set the velocity components as follows:

$$U = 0 \quad V = 0 \quad W = [(\rho W)_{\max}/\rho] \cos(2\pi Ft) \quad (1)$$

where  $F$  is the frequency and  $t$  is the time. With this boundary condition, the density and pressure are extrapolated from the interior of the domain. The  $(\rho W)_{\max}$  was chosen by trial and error in order to achieve an approximate match of the vertical velocity component at the outflow of the orifice with the experiment (the final value used was  $(\rho W)_{\max} = 0.0008\rho_{\infty}a_{\infty}$ , where  $a_{\infty}$  is the reference speed of sound). The resulting  $W$  and  $U$  components of velocity at the orifice exit can be seen in Figs. 2 and 3. Note that use of the current boundary condition fails to capture the sharp peak in  $W$  and the additional hump on the downstroke. Also, it should be noted that the experimental data exhibited significant side ( $V$ -component) velocities during the cycle at this location, whose cause has not been accounted for. The current CFD method makes no attempt to duplicate this  $V$ -velocity component. Also shown in these figures is the effect of fine vs. medium grids, which is very small at this point in the flowfield.

The supplied grid extends .0508 m upstream of center of the orifice, and .1016 m downstream of the center of the orifice. Its height is .076 m above the floor, and its width extends from  $y=-.038$  m to  $+.038$  m

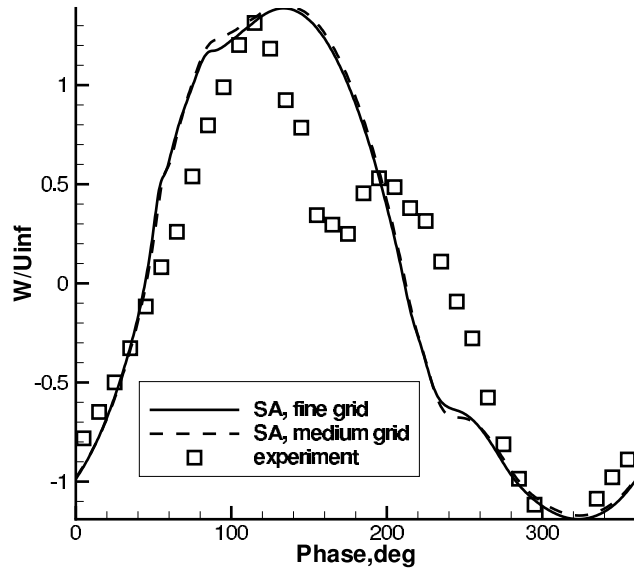


Figure 2: Vertical velocity component at the orifice exit.

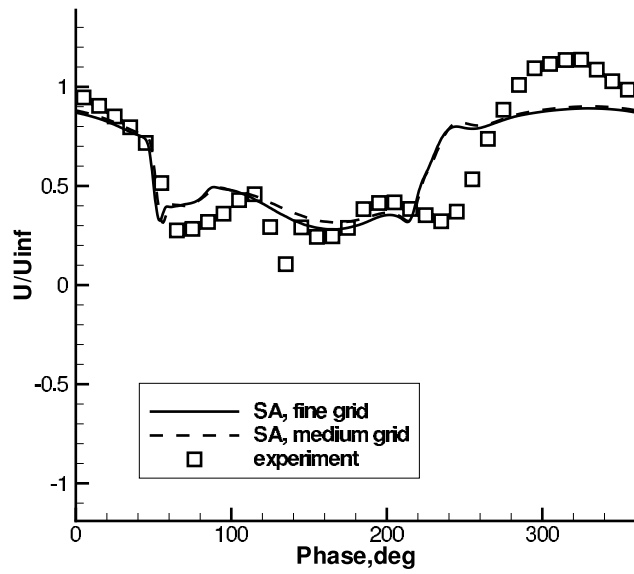


Figure 3: Streamwise velocity component at the orifice exit.

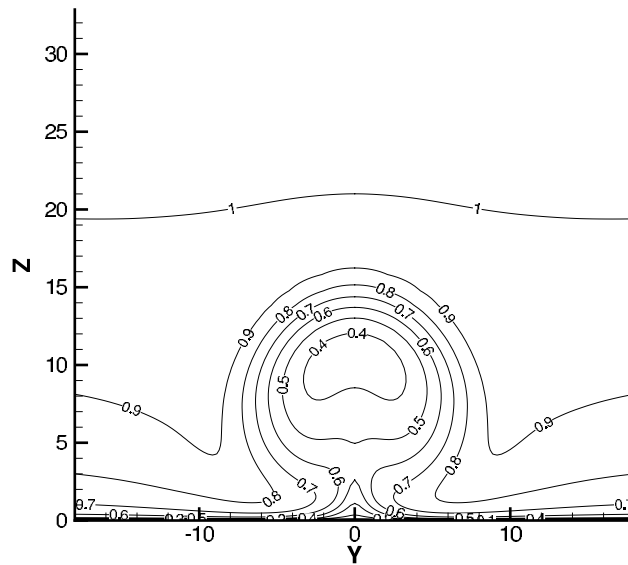


Figure 4: Contours of  $U/U_\infty$  at  $x=76.2$  mm (4D downstream), phase= $200^\circ$ , SA on fine grid.

(total width of .076 m). Note that this height and width are smaller than the wind tunnel height (approx .249 m) and width (.381 m). The boundary conditions at the top, side, and downstream faces of the grid in the tunnel are a farfield Riemann-type. At the upstream face in the tunnel, the density and velocity components are specified in order to approximately match the experimental boundary layer thickness, and the turbulence data is specified in order to approximate a fully-developed turbulent boundary layer in its  $\overline{u'w'}$  component. The pressure at the inflow is extrapolated from the interior of the domain.

Examples of the effects of grid and turbulence model can be seen in Figs. 4, 5, and 6, at phase= $200^\circ$  in the plane 4D downstream ( $x=76.2$  mm). SA on the fine grid yields a somewhat rounder structure than SA on the medium grid, but overall the results are very similar. The differences between the SA and SST models (on the medium grid) are also relatively minor, with the SST model producing a thinner and taller structure.

## References

- [1] Krist, S. L., Biedron, R. T., and Rumsey, C. L., "CFL3D User's Manual (Version 5.0)", NASA TM-1998-208444, June 1998.
- [2] Spalart, P. R., and Allmaras, S. R., "A One-Equation Turbulence Model for Aerodynamic Flows," *La Recherche Aeronautique*, No. 1, 1994, pp. 5–21.
- [3] Menter, F. R., "Two-Equation Eddy-Viscosity Turbulence Models for Engineering Applications," *AIAA Journal*, Vol. 32, No. 8, 1994, pp. 1598–1605.
- [4] Menter, F. R., Rumsey, C. L., "Assessment of Two-Equation Turbulence Models for Transonic Flows," AIAA Paper 94-2343, Colorado Springs, CO, 1994.

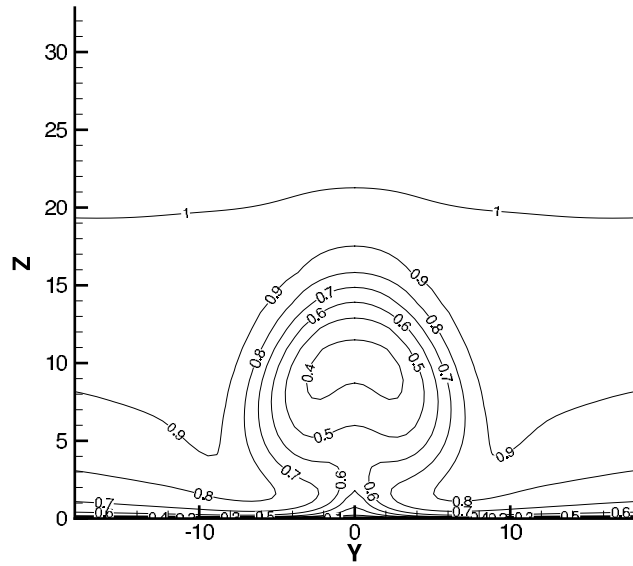


Figure 5: Contours of  $U/U_\infty$  at  $x=76.2$  mm (4D downstream), phase= $200^\circ$ , SA on medium grid.

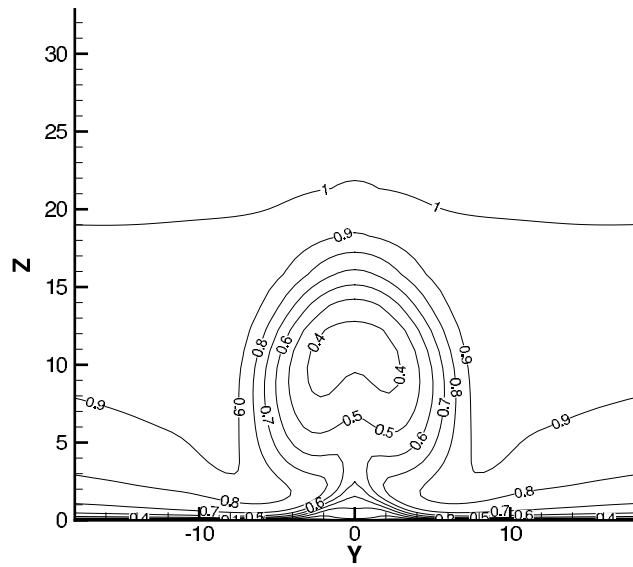


Figure 6: Contours of  $U/U_\infty$  at  $x=76.2$  mm (4D downstream), phase= $200^\circ$ , SST on medium grid.



## CASE 2: SYNTHETIC JET IN A CROSSFLOW

A. Azzi<sup>1</sup>, and D. Lakehal<sup>2</sup>

<sup>1</sup>*Laboratoire de Mécanique Appliquée, Faculté de Génie-Mécanique, Université des Sciences et de la Technologie d'Oran, USTO, BP 1505 El-Mnaouar, Oran, Algeria*

<sup>2</sup>*Institut of Energy Technology, ETH Zentrum/CLT2, CH-8092 Zurich, Switzerland.*

### Solution Methodology

The governing Unsteady Reynolds Averaged Navier Stokes (U-RANS) equations are solved by the use of a three-dimensional finite-volume method that allows the use of arbitrary nonorthogonal grids, employing a cell-centered grid arrangement. A detailed description of the method is reported in Majumdar et al. [1], and the multi-block technique which was introduced afterwards, in Lakehal et al. [2]. The momentum-interpolation technique is used to prevent pressure-field oscillations tending to appear in the cell-centered grid arrangement. The pressure-velocity coupling is achieved by using the well-known SIMPLEC algorithm. The present computations were performed employing the second-order Centered Differential Scheme for all variables applied by a deferred-correction procedure. The resulting system of difference equations was solved using the strongly implicit procedure (SIP) algorithm. The unsteady terms are discretized by an implicit second order time scheme and computations are conducted until a nearly repeating periodic solution is reached. Finally, the long-time-averaged (time-independent mean) values for each quantity are computed as an average over the last period of oscillation.

### Model Description

The Reynolds-stress tensor is approximated within the context of the  $k - \varepsilon$  turbulence model, considering both its linear and nonlinear forms. For the sake of consistency, the two models are coupled with a one-equation model resolving the near-wall viscosity affected regions.

#### The Two-Layer DNS-Based $k - \varepsilon$ Turbulence Model (TLV)

The two-layer approach represents an intermediate modeling strategy between wall function and pure low-Re number models. It consists in resolving the viscosity-affected regions close to walls with a one-equation model, while the outer core flow is treated with the standard  $k - \varepsilon$  model.

The two-layer model used here is a re-formulation of the so-called velocity-scale-based model (TLV) of Rodi et al. [3], in the sense that the turbulent kinetic energy is re-incorporated as a velocity scale. A detailed description of the model is reported in Azzi and Lakehal [4].

#### The EASM model (GSLT)

In this model, the Reynolds stress is represented algebraically in terms of a series of combinations between vorticity and strain. With this, the model is expected to reproduce secondary flows with better accuracy. Although these relationships may be obtained by invoking various strategies, their common starting point is the assumption of homogenous turbulent flows in the limit of equilibrium.

The model used in the present study is a modified version of the EASM model of Gatski and Speziale [5]. In a recent effort to make the model applicable to broad range of practical flows, Lakehal and Thiele [6] emphasized two important aspects: (i) the development of a generalized relation for  $P_k / \varepsilon$ , and (ii) the formulation of a better regularization procedure for  $C_\mu$ .

## Implementation and Case Specific Details

The computational domain is composed by three blocks, including the jet hole and the internal cavity. Only half of the physical domain is computed and a symmetry boundary is applied at  $y=0$  plane. The computational domain extends from -8 diameters upstream to +20 diameters downstream of the centre of the hole. It extends up to 8 diameters over the flat plate in the vertical direction and up to 4 diameters in the spanwise direction (figure 1). A test with 6 diameter in spanwise direction was also tested but gives similar values as with 4d.

Conforming to the guideline instructions, the coordinate system is set with  $x$  downstream,  $z$  up, and  $y$  spanwise, with the  $(x,y,z)=(0,0,0)$  origin at 8 diameters (50.8 mm) directly upstream of the center of the orifice (the orifice diameter is = 6.35 mm).

Results are provided as long-time averaged and phase averaged quantities along specified lines as showed in figure 2.

### Boundary conditions:

The moving diaphragm is represented by an unsteady boundary condition imposed at the bottom side of the cavity. The averaged injected velocity is computed using a blowing ratio of nearly 1, and the unsteady condition is imposed using

$$V = \bar{V} \cos(2\pi \cdot 150 \cdot t) \quad (1)$$

where 150 is the diaphragm frequency.

Preliminary computations have been performed and velocities components at point (50.63 , 0.0 , 0.4) have been found to compare well the averaged data (Figure 3).

The inlet boundary conditions provided in the file (UpstreamBC.dat) are used as mainstream flow inlet conditions. The kinetic turbulent energy is computed according the Reynolds stress components given in

(UpstreamBC.dat) file and its rate of dissipation is computed assuming  $P = \varepsilon$  and  $\varepsilon = u'v' \left[ \frac{\partial U}{\partial y} \right]$ .

A ratio of turbulent to molecular viscosity of 20 is used for injected jet assuming a turbulence intensity of 2%. The time step is fixed at  $dt = 1.852E-5$ , which gives 360 steps per cycle.

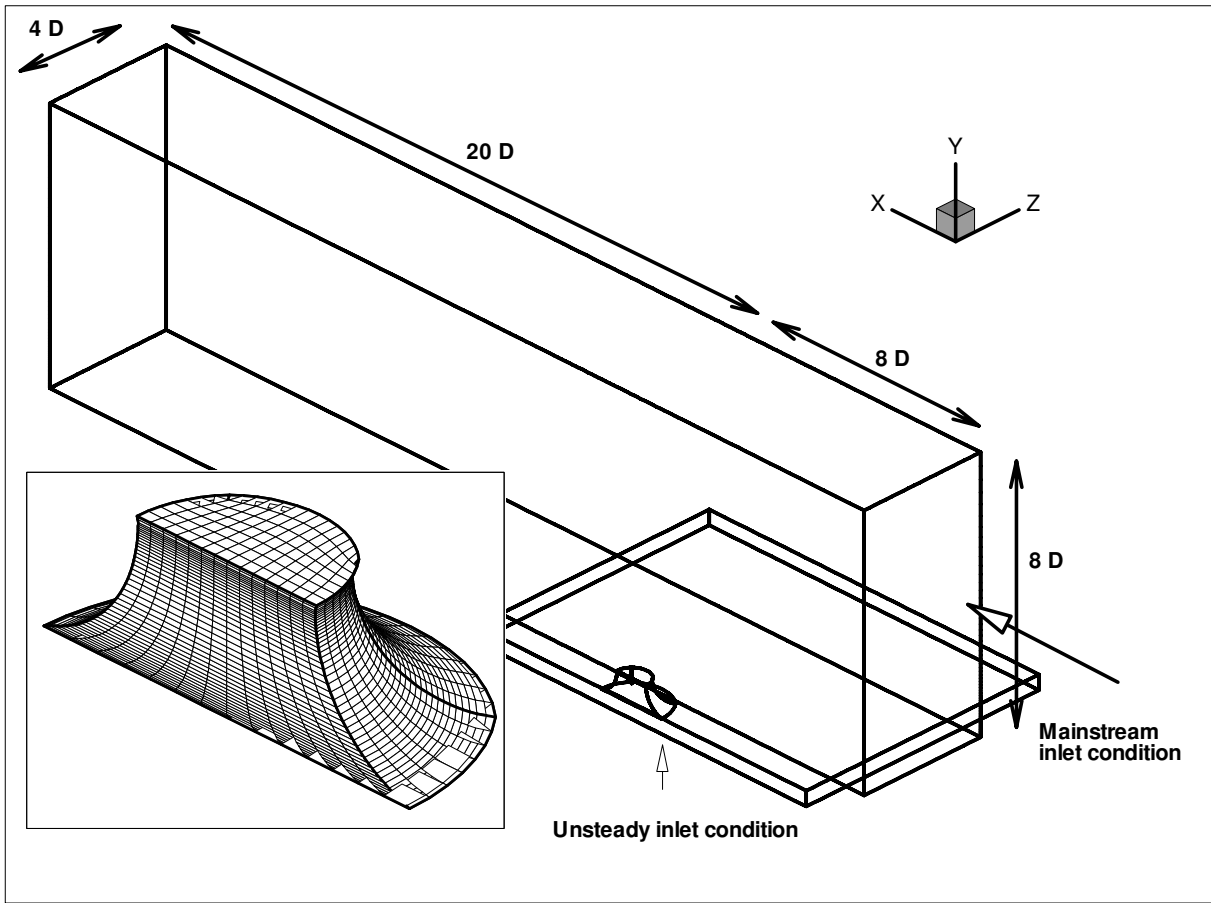


Figure 1: Computational domain and boundary conditions.

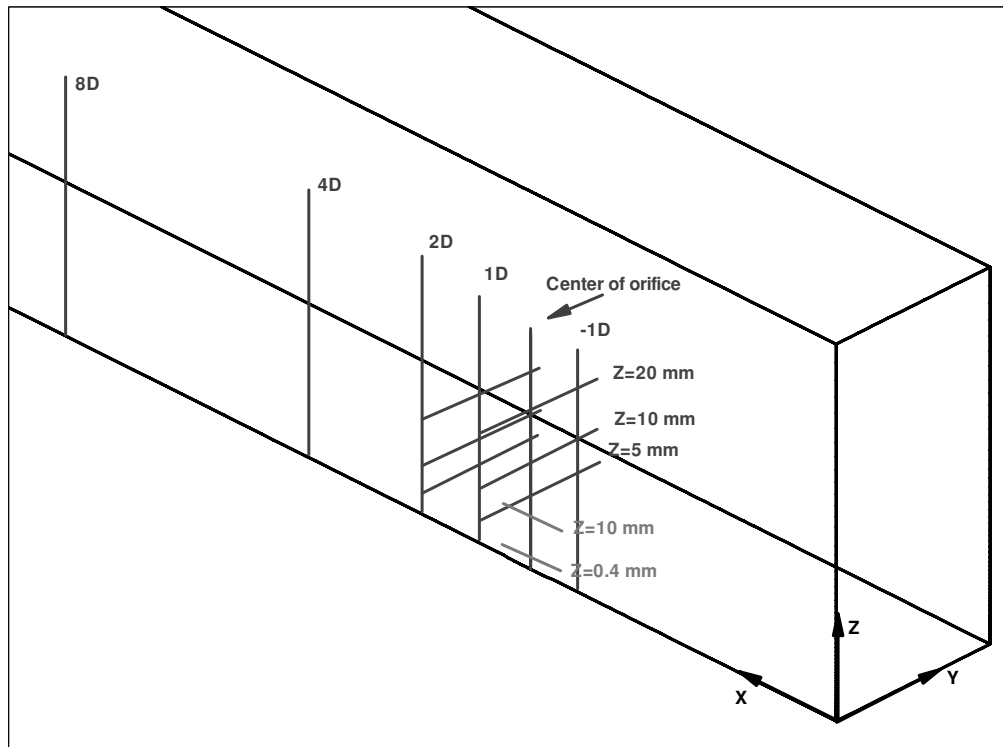


Figure 2: Lines where results are provided.

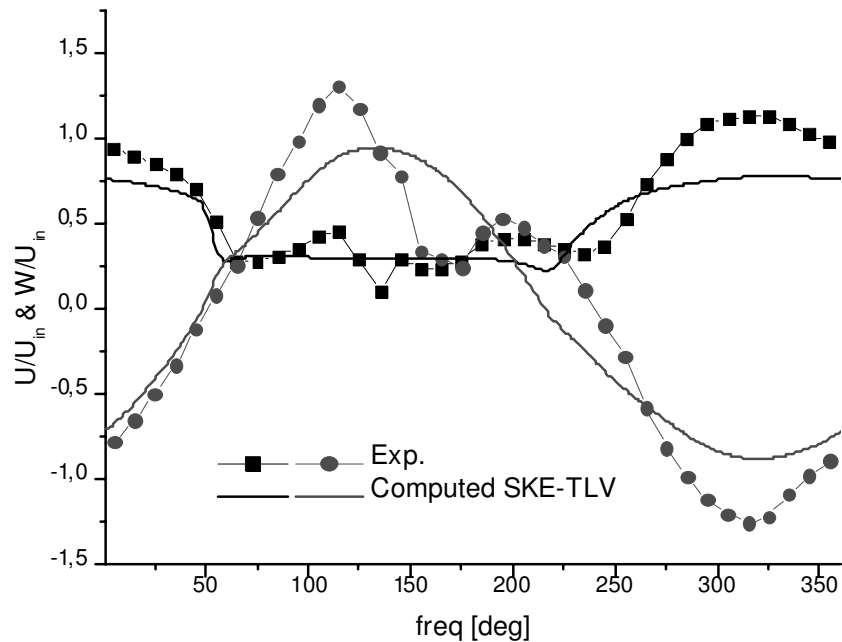


Figure 3: Streamwise and vertical velocities just above the orifice, 0.17 upstream of its centre :  $(x,y,z)=(50.63, 0, 0.4)$  mm

## References

- [1] Majumdar, S., Rodi, W. and Zhu, J. T.B. "Three-Dimensional Finite-Volume Method for Incompressible Flows With Complex Boundaries," *ASME J. Fluids Eng.*, 114, pp. 496-503, 1992.
- [2] Lakehal, D., Theodoridis, G. and Rodi, W. "Computations of Film Cooling of a Flat Plate by Lateral Injection from a Row of Holes," *Int. J. Heat Fluid Flow*, 19, pp. 418-430, 1998.
- [3] Rodi, W. Mansour, N. N. and Michelassi, V. "One-Equation Near Wall Turbulence Modelling with the Aid of Direct Simulation Data," *ASME J. Fluids Eng.*, 115, pp. 196-205, 1993.
- [4] Azzi, A. and Lakehal, D. "Perspectives in Modeling Film Cooling of Turbine Blades by Transcending Conventional Two-Equation Turbulence Models," *EASM J. of Turbomachinery*, 124, pp. 472-484, 2002.
- [5] Gatski, T. B. and Speziale, C. G. "On Explicit Algebraic Stress Models for Complex Turbulent Flows," *J. Fluid Mech.*, 254, pp. 59-78, 1993.
- [6] Lakehal, D. and Thiele, F. "Sensitivity of Turbulent Shedding Flows Part Cylinders to Non-Linear Stress-Strain Relation and Reynolds Stress Models," *Comput. Fluids*, 30, pp. 1-35, 2001.

# **CASE 2: SIMULATION OF A PERIODIC JET IN A CROSS FLOW WITH A RANS SOLVER USING AN UNSTRUCTURED GRID**

H. L. Atkins

*Computational Modeling & Simulation Branch, NASA Langley Research Center, Hampton, VA 23681-2199*

## **Introduction**

A second-order unstructured-grid code, developed and used primarily for steady aerodynamic simulations, is applied to the synthetic jet in a cross flow. The code, FUN3D, is a vertex-centered finite-volume method originally developed by Anderson[1, 2], and is currently supported by members of the Fast Adaptive Aerospace Tools team at NASA Langley. Used primarily for design[3] and analysis[4] of steady aerodynamic configurations, FUN3D incorporates a discrete adjoint capability, and supports parallel computations using MPI.

## **Solution Methodology**

A detailed description of the FUN3D code can be found in the references given above. The code is under continuous development and contains a variety of flux splitting algorithms for the inviscid terms, two methods for computing gradients, several turbulence models, and several solution methodologies; all in varying states of development. Only the most robust and reliable components, based on experiences with steady aerodynamic simulations, were employed in this work.

As applied in this work, FUN3D solves the Reynolds averaged Navier-Stokes equations using the one equation turbulence model of Spalart and Allmaras[5]. The spatial discretization is formed on unstructured meshes using a vertex-centered approach. The inviscid terms are evaluated by a flux-difference splitting formulation using least-squares reconstruction and Roe-type approximate Riemann fluxes. Green-Gauss gradient evaluations are used for viscous and turbulence modeling terms.

The discrete spatial operator is combined with a backward time operator which is then solved iteratively using point or line Gauss-Seidel and local time stepping in a pseudo time. For steady flows, the physical time step is set to infinity and the pseudo time step is ramped up with the iteration count. A second-order backward in time operator is used for time accurate flows with 20 to 50 steps in the pseudo time applied at each physical time step.

For this effort, FUN3D was modified to support spatially varying boundary and initial conditions, and unsteady boundary conditions. Also, a specialized in/out flow boundary condition was implemented to model the action of the diaphragm. This boundary condition is described below in more detail.

The grids were generated using the internally developed codes GridEX[6] for meshing the surfaces and inviscid regions of the domain, and for CAD access; and MesherX[7] for meshing the viscous regions. Grid spacing in on the surfaces and in the inviscid regions are indirectly controlled by specifying sources. The viscous layers are generated using an advancing layer technique. MeshersX allows the user to control the spatial variation of the first step off the surface, growth rates, and the termination criterion by providing small problem dependent subroutines.

## **Modeling of Diaphragm Boundary**

A specialized in/out flow boundary condition is formulated to model the action of the diaphragm at a stationary boundary. This boundary condition is similar to a standard characteristic boundary condition, commonly

applied at far-field boundaries, in that the inviscid boundary flux is evaluated from an intermediate solution state  $U_i$  that is computed from the current boundary solution  $U_b$  and a prescribed external state  $U_p$ . In the weak form implemented in FUN3D, the boundary solution is not replaced by the intermediate solution but is allowed to evolve. The viscous gradients are evaluated using only the boundary and interior solution values, and have no knowledge of the prescribed or intermediate solution states.

At a far-field boundary, the intermediate solution is determined by the characteristic relationships that model the convective and acoustic waves that are assumed to exist between the boundary and the far-field. For example, at a subsonic boundary

$$R^+(U_i) = R^+(U_b), \quad R^-(U_i) = R^-(U_p), \quad \text{and} \quad R_c(U_i) = \begin{cases} R_c(U_b) & \text{if } V_n \geq 0 \\ R_c(U_p) & \text{otherwise,} \end{cases} \quad (1)$$

where  $R^+(-)$  denotes the characteristic variable associated with acoustic waves leaving(entering) the domain,  $R_c$  denotes characteristic variables associated with convective waves, and  $V_n$  is the normal velocity through the boundary, with outflow taken as positive.

In the case of a moving diaphragm, the ‘‘prescribed’’ state is that at the diaphragm face, and only the diaphragm velocity is known. If the boundary were moving with the diaphragm, than the intermediate state would be given by

$$V_n = 0, \quad R^+(U_i) = R^+(U_b), \quad \text{and} \quad R_c(U_i) = R_c(U_b). \quad (2)$$

Simply applying these conditions at a stationary location, by setting  $V_n$  equal to the diaphragm velocity, would result in under specifying the flow during the inflow phase of the simulation. To stabilize the simulation, the latest value of  $R_c$  is saved during the outflow phase of the calculation, and reapplied during the inflow phase to give:

$$V_n = \alpha \cos(\omega t), \quad R^+(U_i) = R^+(U_b), \quad \text{and} \quad R_c(U_i) = \begin{cases} R_c(U_b) & \text{if } V_n \geq 0 \\ \hat{R}_c(U_b) & \text{otherwise,} \end{cases} \quad (3)$$

where  $\hat{R}_c$  denotes the value saved from the most recent outflow cycle. In practice, only the entropy is saved and reapplied. The boundary tangential velocity is allowed to evolve without constraint. Also, during the inflow cycle, the entropy is gradually relaxed back toward its initial value.

## Implementation and Case Specific Details

The geometry of the cavity is simplified by making the diaphragm flat with the height of the diaphragm chosen so that the ‘‘at rest’’ volume of the cavity is unchanged. To reduce the problem size, the domain is divided at the tunnel centerline and only half of the domain is grided. Although all simulations presented here were performed on this half-domain geometry, it is possible to reflect the grid about the centerline to obtain a symmetric grid for the larger problem. The computational domain extends from 8 jet diameters upstream and to the side of the jet center, and to 16 jet diameters downstream of the jet center.

The fine grid was sized so that the first spacing on the tunnel wall would have a  $y^+ \leq 1$ . Spacings inside the cavity were based on preliminary simulations with steady blowing applied at the diaphragm face. Griding sources were placed around the lip of the jet and along the jet centerline in an effort to improve the clustering there. Figures 1(a-c) shows three views of the mesh on the symmetry plane that illustrate the mesh distribution near the jet.

A coarse grid was generated simply by doubling all grid sources and modifying the growth rate of the viscous layers. Originally, this grid was intended only to provide rapid turn-around while sorting out boundary and initial conditions. The fine grid has 1457853 tetrahedra and 255426 nodes. The coarse grid has 254046 tetrahedra and 46063 nodes.

Characteristic boundary conditions are applied weakly at the inflow, outflow and top boundaries. Symmetry conditions are imposed at both  $y=\text{constant}$  boundaries. No-slip conditions are enforced on the tunnel

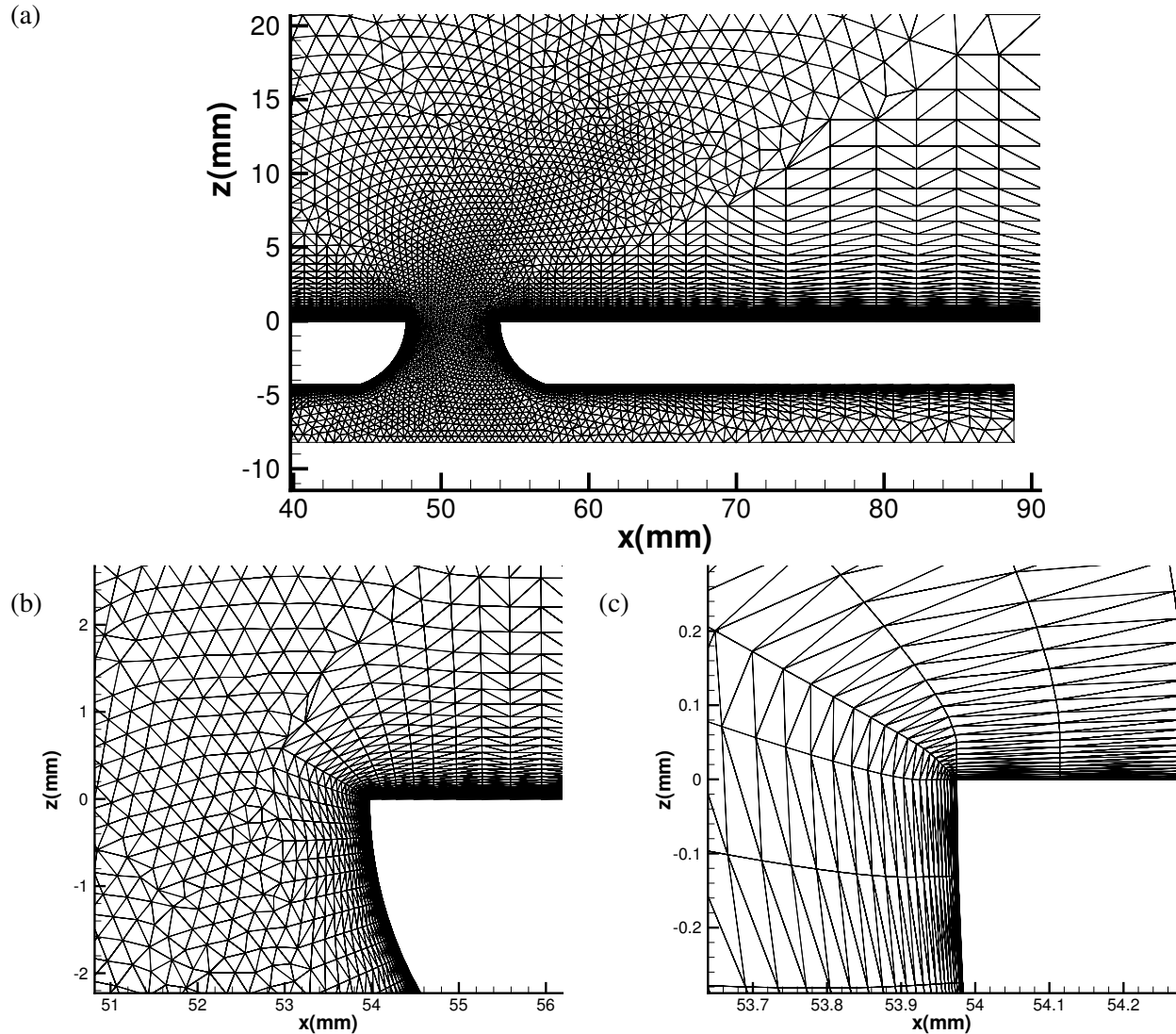


Figure 1: Grid on the symmetry plane: a) overall view, b) near jet exit, c) near corner of jet exit.

floor, the top wall of the cavity, and in the jet contraction. At these no-slip boundaries, the temperature is set to the adiabatic wall temperature, and the density is determined from the continuity equation. The side walls of the cavity are treated as inviscid walls, which FUN3D enforces weakly. The in/out flow boundary condition described in the previous section is applied on the lower wall of the cavity.

The inflow and initial conditions in the tunnel region were generated by performing a separate boundary layer simulation with FUN3D and extracting the solution at the appropriate Reynolds number. Initially, there is no flow in the cavity and the pressure is set to the freestream value. The simulation was started impulsively with the diaphragm velocity (normalized by  $u_\infty$ ) specified as  $-0.007 \cos(\omega t)$ . The simulations used 720 time steps per period, with results saved every 5 degrees of phase. The long time averages requested by the workshop were computed by averaging these 5-degree samples. The fine grid simulations required 35 hours per period when using 16 intel processors; the coarse grid simulations required less than 11 hours per period when using 8 processors.

The fine and coarse grid simulations produced noticeably different solutions in several respects. Figures 2 (a) and (b) show the fine grid solution history at a location 0.17mm upstream of the jet center. Although the vertical velocity component  $W$  settles quickly to a periodic solution, the streamwise velocity

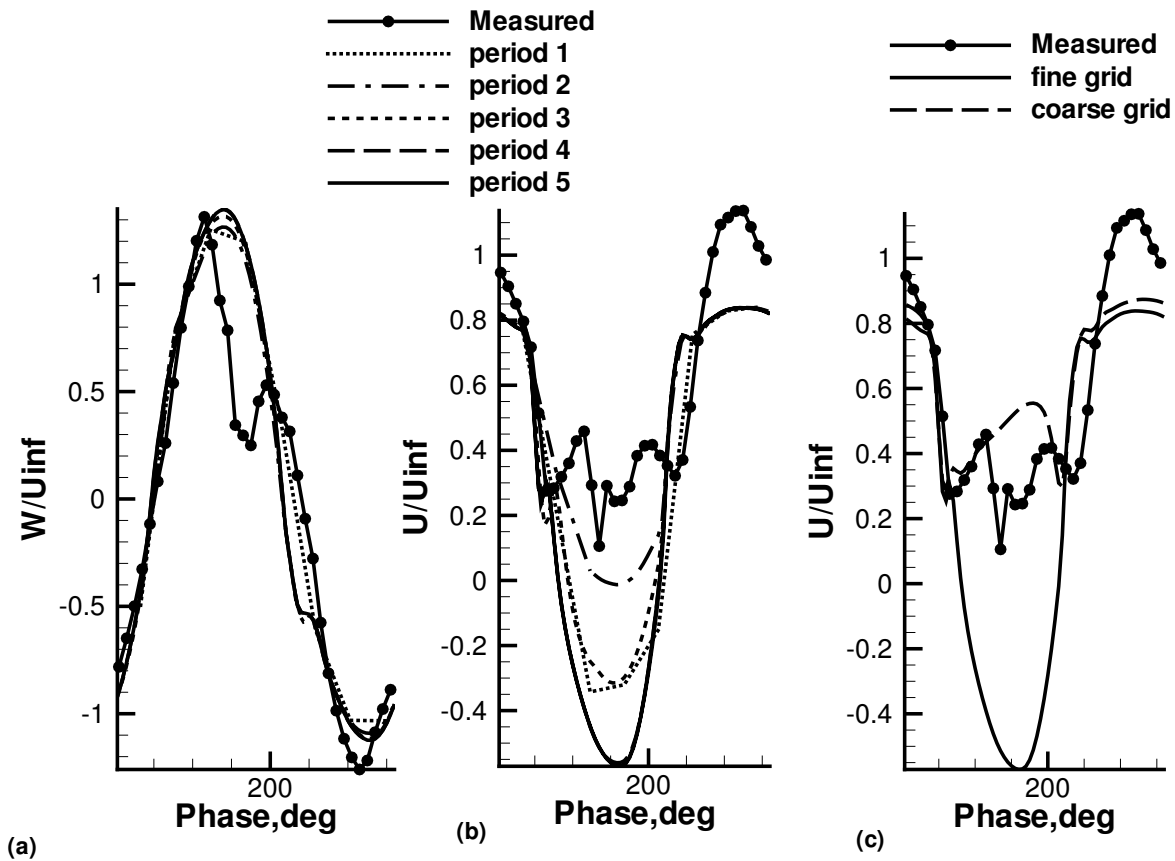


Figure 2: Solution at 0.17mm upstream of jet center: a) and b) fine grid startup history of  $W$  and  $U$ , respectively; c) comparison of  $U$ .

component  $U$  requires 4 periods. In the coarse grid simulation, the solution requires even longer, 6 periods, before the  $U$  velocity component becomes periodic. The fine and coarse grid simulations give similar results for  $W$ , but the  $U$  velocity components, compared in fig. 2(c), have completely different character during the blowing phase. The coarse grid produces results similar to the experiment, while the fine grid predicts a large negative streamwise velocity component during the blowing cycle. The contour plots of  $U$ , shown in fig. 3, indicate that this negative streamwise velocity is due to a vortical behavior that develops in the jet exit flow.

## Acknowledgments

The author would like to acknowledge Bill Jones and Mike Park for their assistance and suggestions with grid generation, and Bob Biedron, Beth Lee-Rausch and Eric Nielson for their assistance and advice in modifying and running FUN3D.

## References

- [1] Anderson, W. Kyle and Bonhaus, Daryl L. "An Implicit Upwind Algorithm for Computing Turbulent Flows on Unstructured Grids," *J. Computers and Fluids*, Vol. 23, No. 1, pp. 1–21, 1994.

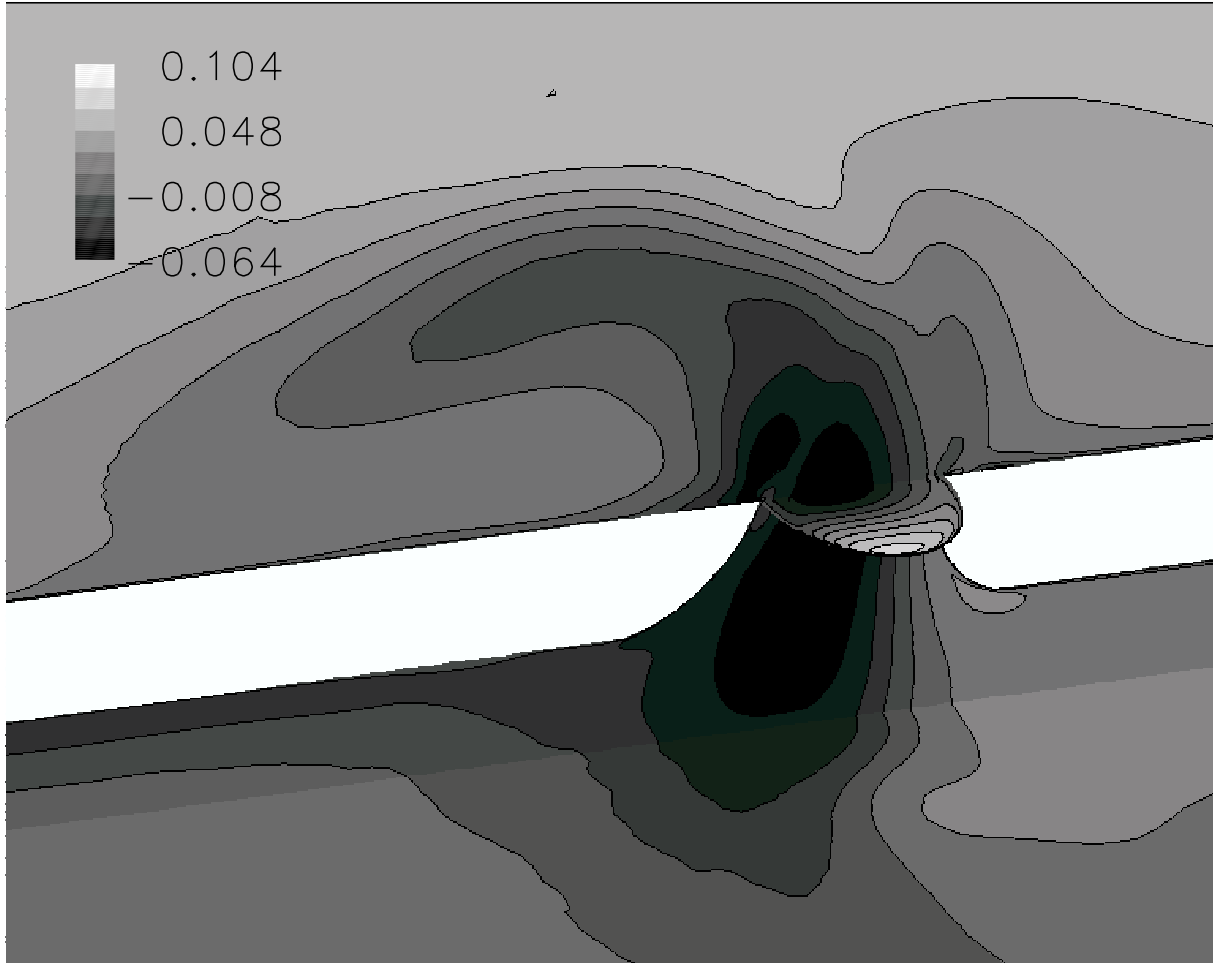


Figure 3: Streamwise velocity contours from fine grid simulation during peek blowing: phase = 160.

- [2] Anderson, W. K. and R. D. Rausch and Bonhaus, D. L. "Implicit/Multigrid Algorithms for Incompressible Turbulent Flows on Unstructured Grids," *J. Computational Physics*, Vol. 128, pp. 391-408, 1996.
- [3] Neilson, Eric, J. and Lu, James and Park, Mike A. and Darmofal, David L "An Exact Dual Adjoint Solution Method for Turbulent Flows on Unstructured Grids," AIAA paper 2003-0272, 2003, to appear in *J. Computers and Fluids*.
- [4] Lee-Rausch, E. M. and Mavriplis, D. J. and Rausch, R. D. "Transonic Drag Prediction on a DLR-F6 Transport Configuration Using Unstructured Grid Solvers," AIAA Paper 2004-0554, 2004.
- [5] Spalart, P. R. and Allmaras, S. R. "A One-Equation Turbulence Model for Aerodynamic Flows," AIAA paper 92-0429, 1992.
- [6] Jones, William T. "GridEx - An Integrated Grid Generation Package for CFD," Proceedings of the 16th AIAA Computational Fluid Dynamics Conference, AIAA Paper 2003-4129, 2003.
- [7] Park, Micheal A. "Three-Dimensional Turbulent RANS Adjoint-Based Error Correction," AIAA paper 2003-3849, 2003.



# **CASE 2: 3D NUMERICAL SIMULATION OF SYNTHETIC JET IN A CROSSFLOW USING A PARALLEL UNSTRUCTURED INCOMPRESSIBLE NAVIER-STOKES SOLVER**

V. K. Parimi, H. Chen, L. Huang, V. Katam, R. P. LeBeau, and P .G. Huang

*Department of Mechanical Engineering, University of Kentucky, Lexington, KY 40506-0108*

## **Introduction**

Active flow control technologies is growing area of aerodynamic research in the early 21<sup>st</sup> century. The goal is to prevent boundary layer separation and as such it is often applied to designs of high-lift airfoils. Forced oscillations superimposed on a mean flow which is on the verge of separation point is an effective means to delay boundary-layer separation, such as blowing or suction techniques. However, the progress in active flow control technologies has often been paced by the development of actuator capabilities. A popular current actuator is the synthetic jet, which has demonstrated capabilities regarding separation control and thrust vectoring.

Over the past several decades, both computational fluid dynamics (CFD) algorithms and computer technologies have progressed tremendously. These advances have made unstructured grids more attractive with their ability to smoothly conform to varying flow conditions and complicated boundaries with a single grid. However, challenges remain, including grid generation for a computational domain with complex geometries, well-balanced grid decomposition on distributed system, and efficient parallel performance. In this paper, a 3D numerical simulation of a synthetic jet into a cross flow using a new CFD code called UNCLE is described. UNCLE is a 2D/3D finite volume unstructured unsteady incompressible Navier-Stokes solver. In order to take care of turbulence flow in most realistic cases, F. R. Menter's shear-stress transport (SST) turbulence model [1] is employed to UNCLE. It is designed to study the challenges of using unstructured grid codes on high-performance parallel computers to simulate realistic cases. To increase flexibility in complex geometries, UNCLE may use a variety of grid types, such as triangles, quadrilateral, tetrahedron and hexahedra meshes. In order to achieve good load balance for parallel computing, METIS [2] is used to partition the grid.

## **Solution Methodology**

UNCLE employs a pressure-based SIMPLE algorithm with second order accuracy in both time and space. A second order upwind scheme is used for computing advection terms. Non-staggered grids with the Rhie and Chow momentum interpolation method [3] are employed to avoid checkerboard solutions. In order to take care of turbulence flow in most realistic cases, F. R. Menter's shear-stress transport (SST) turbulence model [1] is implemented. It is designed to study the challenges of using unstructured grid codes on high-performance parallel computers to simulate realistic cases. To increase flexibility in complex geometries, UNCLE may use a variety of grid types, such as triangles, quadrilateral, tetrahedron and hexahedra meshes.

In order to achieve good load balance for parallel computing, METIS [2] is used to partition the grid. Generally, there are two different partitioning approaches – vertex based and element based partitioning for mesh-partitioning as shown in Fig. 1(a) and (b) respectively. For vertex-based partitioning, the boundary elements are doubled and the vertices at the boundary are overlapped. Since the control volumes at boundary are not partitioned, only communication of boundary nodal properties is required. For element-based partitioning, the boundary vertices are

doubled. Because the control volumes at the boundary are split, all nodal points surround a boundary vertex are needed to interpolate the properties of the boundary vertices. Communication of boundary nodal properties in element based partitioning is heavier than vertex-based partitioning. On the other hand, vertex-based partitioning has to handle doubled elements at the boundary, it still costs computational time. For the purpose of direct use the information from METIS, element based partitioning is used for pre-processing code of UNCLE.

## Model Description

F. R. Menter's SST turbulence model [1] is employed in this simulation.

## Implementation and Case Specific Details

In this case, the orifice diameter, 6.35 mm is chosen to be the reference length. Air density at sea level is  $1.185\text{kg/m}^3$ , viscosity is  $18.4\text{e-}6\text{kg/m-s}$ , and the reference velocity is the freestream velocity which is  $34.6\text{m/s}$ . According to the information above, the Reynolds number for this case is 1414.8.

We assume the flow is symmetric about  $y = 0$  plane, so only half of the experimental domain is used as the computational domain. An unstructured grid is generated to fulfill the grid format of UNCLE by using GAMBIT. The total grid has 0.3 million cells. The geometry of the grid is similar to the provided grids from the cfdval2004 website

In order to simulate the moving diaphragm, a periodic velocity boundary condition is used to replace moving boundary condition. The non-dimensional period  $T$  can be calculated by:

$$1/T = f^* = f * \ell / u \quad (1)$$

where  $f^*$  is non-dimensional frequency, frequency  $f = 150\text{Hz}$ , reference length  $\ell = 0.00635\text{ m}$ , and reference velocity  $u = 34.6\text{ m/s}$ . As a result of eq. (1), the non-dimensional period  $T$  is 36.325 approximately. Using the driver's boundary conditions from the experimental data provided on the cfdval2004 website, the velocity at the center of the diaphragm is obtained. The time-dependent velocity at the center of the diaphragm can be approximated by curve-fitting method, and its mathematical formulation is described as:

$$w(t) = a + b * \cos(c * t + d), \quad (2)$$

$$a=2.642281\text{e-}6, b=0.020915027, c=0.17405397, d=-0.027378007$$

where  $a$ ,  $b$ ,  $c$ , and  $d$  are dimensionless parameters and  $t$  is dimensionless time. Symmetry boundary condition is used along the symmetry plane. For the rest of the boundary, the no-slip condition is imposed as the wall boundary condition. In this simulation, the non-dimensional time for one step is chosen as 0.009 so that the total number of time steps for each cycle is 4036.

## References

1. Menter, F. R., "Two-Equation Eddy-Viscosity Turbulence Models for Engineering Applications," *AIAA Journal*, Vol. 32, No. 8, pp. 1598-1605, 1994.
2. Karypis, G. and Kumar, V., "A software package for partitioning unstructured graphs, partitioning meshes, and computing fill-reducing orderings of sparse matrices version 4.0," <http://www.cs.umn.edu/~karypis>, 1998.
3. Rhie, C. M. and Chow, W. L., "Numerical study of the turbulent flow past an airfoil with trailing edge separation," *J. AIAA*, 21, pp. 1525-1532.

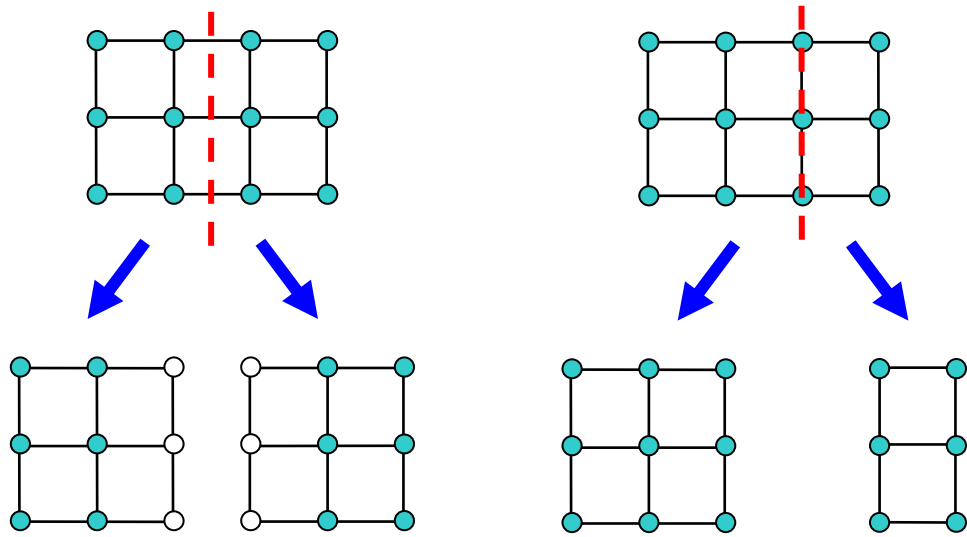


Fig. 1(a) Schematic of vertex based partitioning, (b) Schematic of element based partitioning.



# CASE 2: Lumped Element Modeling of a Zero-Net Mass Flux Actuator Interacting with a Grazing Boundary Layer

Quentin Gallas,<sup>§</sup> Rajat Mittal,<sup>‡</sup> Mark Sheplak<sup>†</sup> and Louis Cattafesta<sup>†</sup>

<sup>§†</sup>Department of Mechanical & Aerospace Engineering, University of Florida, Gainesville, FL 32611-6250

<sup>‡</sup>Department of Mechanical & Aerospace Engineering, George Washington University, Washington, DC 20052

<sup>§</sup>Graduate Student

<sup>†‡</sup>Associate Professor

## Introduction

The approach described here is to model the response of a synthetic jet to a grazing boundary layer using lumped element modeling. This effort complements more rigorous and expensive numerical simulations.

## Solution Methodology

The approach used is to model the actuator orifice impedance with a grazing boundary layer and is based on a lumped element modeling (LEM) technique, following the recent paper by Gallas et al. [1].

## Model Description

For a full discussion on the LEM technique used herein, the reader is referred to the write-up for Case 1 and to the details and references contained in Gallas et al. [1]. In summary, in LEM the individual components of a synthetic jet are modeled as elements of an equivalent electrical circuit using conjugate power variables (i.e., power = generalized “flow” x generalized “effort” variables); the lumped parameters represent generalized energy storage elements (i.e., capacitors and inductors) and dissipative elements (i.e., resistors), as shown in Figure 1. The frequency response function of the circuit is then derived to obtain an expression for  $Q_{out}$ , the volume flow rate. LEM provides a compact nonlinear analytical model and valuable physical insight into the dependence of the device behavior on geometry and material properties.

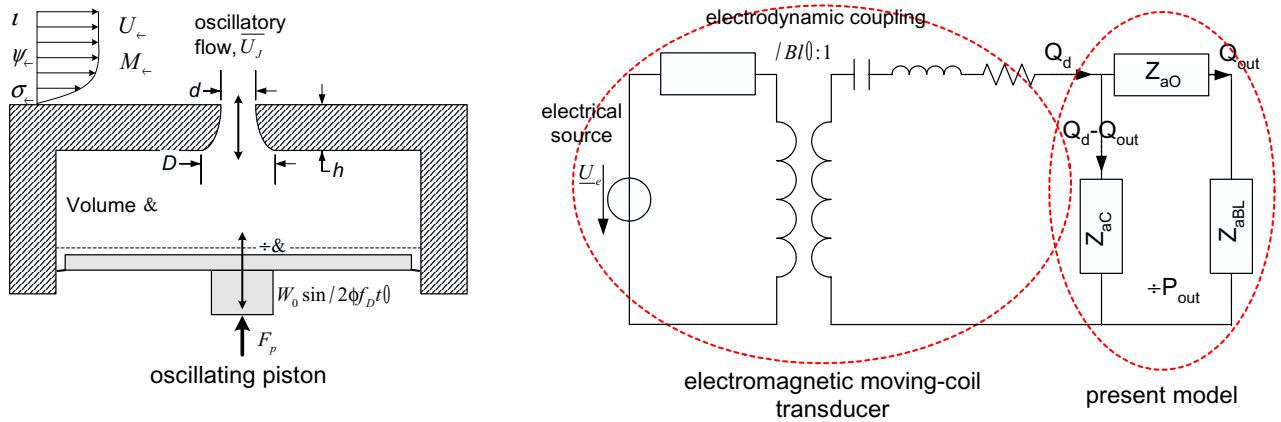


Figure 1: Equivalent circuit of an electrodynamic synthetic jet with a crossflow BL.  $Z_{aC} = \rho c / (4Q_{out})$  is the cavity acoustic impedance,  $Z_{aO} = 2Z_{aBL} = \rho c / (Q_{out})$  is the orifice acoustic impedance.

Case 2 is similar to the device studied and modeled by Gallas et al., although now the driver is a voice-coil driven piston, and the synthesized jet interacts with a crossflow boundary layer. No information is

available about the dynamics of the electromagnetic transducer. Instead, the measured sinusoidal displacement of the (assumed) rigid piston is used to calculate the piston volume velocity

$$Q_d = j\omega \Delta V = j\omega S_d W_0 \sin(\omega t) \quad (1)$$

where  $\Delta V$  represents the volume displaced by the piston,  $S_d$  is the effective moving area of the piston and  $W_0$  is the amplitude of oscillation of the piston. This representation enables us to bypass the need of an expression for the impedance of the transducer shown in Figure 1.

The model considered and developed in [1] is for a device exhausting into a quiescent medium. Thus, in order to account for the incoming crossflow effect, a boundary layer impedance is introduced in series with the orifice impedance since they share the same volume flow  $Q_{out}$ . The work done in the acoustic liners community has been used to derive a simple analytical expression for this grazing impedance. Specifically, it is derived from the boundary conditions used in the so-called NASA Langley Zwikker-Kosten Transmission Line Code (ZKTL), which finds its origins in the work done by Hersh and Walker [2], Heidelberg [3] and Motsinger and Kraft [4]. With slight modifications and rearrangement, the model is extended for the present problem to yield the following impedance model in the acoustic domain

$$Z_{aBL} = R_{aBL} + jX_{aBL} \quad (2)$$

where the acoustic resistance and reactance contribution from the crossflow boundary layer are, respectively

$$R_{aBL} = \frac{\psi c_0}{S_n} \frac{M_\infty}{2.2 \cdot 1.256 \sqrt{d}} \quad \text{and} \quad X_{aBL} = \frac{\psi c_0}{S_n} \frac{2\phi f}{c_0 C_D} \frac{0.85d}{1.2 \cdot 305 M_\infty^3} \quad (3)$$

where  $j = \sqrt{-1}$ ,  $\psi$  is density,  $S_n$  is the orifice exit area,  $C_D$  is the orifice discharge coefficient defined below,  $d$  is the exit orifice diameter,  $\tau$  is the boundary layer thickness,  $f$  is frequency,  $c_0$  is the isentropic speed of sound, and  $M_\infty$  is the freestream Mach number. Note that this boundary layer impedance model is primarily a function of the Mach number and of the ratio of the orifice diameter to the boundary layer thickness. The main contribution of the crossflow is to increase the resistance of the orifice and to reduce the effective mass oscillating in the orifice. This model does not provide detailed information on how the velocity profile is skewed by the grazing flow.

The acoustic impedance of the orifice is given by the following expression, where again analytical expressions for each lumped parameter are provided in [1],

$$Z_{aO} = R_{aOlin} + 2 R_{aOnl} + j\omega M_{aO} \quad (4)$$

Because of the particular shape of the orifice (aspect ratio  $h/d < 1$ , beveled orifice), the linear resistance  $R_{aOlin}$  due to the viscous losses will be small compared to the nonlinear ‘‘dump’’ loss effects that are represented by a nonlinear resistance  $R_{aOnl}$ . This term is modeled as a generalized Bernoulli flow meter and is given by

$$R_{aOnl} = \frac{\psi K_D Q_{out}}{2S_n^2} \quad (5)$$

where the dump loss coefficient for the orifice is  $K_D = \left( \sqrt{1.4} \eta^4 / C_D \right)^{4.2}$ , with  $\eta = d/D$  the ratio of the exit to the entrance orifice diameter, and with the discharge coefficient  $C_D = 0.9975 - 4.653/\eta / \text{Re}_d^{0.5}$ ,  $\text{Re}_d$  being the Reynolds number based on the orifice exit diameter. For the current configuration, we find that  $K_D \approx 1$ .

Finally, from Figure 1 the expression for the jet volume flow rate during the expulsion part of the cycle can be written in the following form (see Case 1 write-up and [1] for variable definitions):

$$Q_{out} = Q_d \frac{Z_{aC}}{Z_{aC} + 2Z_{aO} + 2Z_{aBL}} \frac{s + \&}{s^2 C_{aC} / M_{aO} + 2M_{aBL} + 2s C_{aC} / R_{aOlin} + 2R_{aOnl} + 2R_{aBL}} \quad (6)$$

For an oscillatory channel flow in a circular duct, as discussed in [1], the ratio of the average velocity to the centerline velocity is strongly influenced by the Stokes number. Since, for the present case, the Stokes number  $S = \sqrt{2\phi f d^2 / \tau} = 49.47$ , the ratio is estimated as  $u_{avg} / u_{CL} = 0.9$ , where  $u_{avg}$  corresponds to the spatially averaged velocity during the ejection portion of one cycle, and  $u_{CL}$  is the centerline velocity. Therefore, since LEM gives the volume flow rate through the orifice, the centerline velocity is

$$u_{CL} = \frac{Q_{out}}{\phi / d / 20^2 / 0.90} \quad (7)$$

## Implementation and Case Specific Details

In the approach considered above, the main difficulty comes from the proper modeling of the driver volume velocity and cavity volume. Indeed, in this modeling technique the output flow is highly dependant on the driver dynamics, especially since at low frequencies,  $s = j\omega \downarrow 0$ , Eq. (6) shows that the response is governed by  $Q_d$ . It is unclear, however, whether the effective moving area  $S_d$  of the driver is constituted by only the rigid piston or if the flexible membrane displaces some fluid. From a simple control volume analysis, assuming incompressible flow and equating the volume fluxes gives

$$|Q_d| = 2\phi S_d W_0 = u_{CL} S_n / 0.90 = |Q_{out}| \quad (8)$$

Substituting in the experimental values that are provided and solving for  $S_d$  yields an effective area of the driver  $S_d = u_{CL,exp} S_n / 0.90 / 2\phi W_0 = 1748.5 \Delta 10^{-6} \text{ mm}^2$ , which is much less than the value computed from the drawings provided on the web site when considering the flexible membrane as a “tensioned drum” ( $S_d = 4076.7 \text{ mm}^2$ ). A careful analysis of the piston/membrane dynamics is required to assess the severity of this issue. Nevertheless, for the present time, we assume that only the rigid piston displaces the fluid, with an area of  $2570.4 \text{ mm}^2$ .

Another point is that the piston-diaphragm is assumed to oscillate in a sinusoidal motion, which turns out to be not quite true when comparing the piston displacement over one cycle with a pure sine wave. This is actually not unexpected, but it emphasizes the need to model the entire electromagnetic transducer.

Also, the LEM analysis above can assess the validity of assuming incompressible flow inside the cavity. The drive frequency is 150 Hz; it can be shown that a requirement for the incompressibility limit inside the cavity is that the operating frequency of the actuator should be much less than the Helmholtz frequency. Here the Helmholtz frequency is

$$f_H = \frac{1}{2\phi} \frac{1}{\sqrt{C_{aC} / M_{aO} + 2M_{aBL}}} = 614 \text{ Hz} \quad (9)$$

Next, in order to further characterize the response of the system and to fully understand the effect of the nonlinearity present in the orifice resistance, a time domain analysis is performed on the actuator from the circuit shown in Figure 1.

The equation of motion of a fluid particle  $x_{out}$  is easily derived and is given by a nonlinear 2<sup>nd</sup>-order oscillator equation

$$\frac{1}{M_{aO}} \left( 2 M_{aBL} \ddot{x}_{out} + 2 R_{aOnl} \dot{x}_{out} + \frac{2}{R_{aOlin}} \frac{1}{2 R_{aBL}} \dot{x}_{out} + \frac{1}{C_{aC}} x_{out} \right) = \frac{S_d}{C_{aC} S_n} W_0 \sin(\omega t). \quad (10)$$

Similarly, the pressure across the orifice is given by

$$\dot{P}_{out} = \frac{S_d}{C_{aC}} W_0 \sin(\omega t) - 4 \frac{S_n}{C_{aC}} x_{out}. \quad (11)$$

The ODE that describes the motion of the fluid particle at the orifice is numerically integrated using a 4<sup>th</sup> order Runge-Kutta method with zero initial conditions. The integration is carried out until a steady-state is reached. The jet orifice displacement and velocity, pressure drop across the orifice, and the driver displacement are shown in Figure 2 for both the (a) linear and the (b) nonlinear solutions of the equation of motion. The linear solution is obtained by setting  $R_{aOnl} = 0$  and is performed to verify the physics of the device behavior and thus confirm the modeling approach used. The linear solution in Figure 2a shows that the pressure inside the cavity (which = the pressure across the orifice  $\dot{P}_{out}$ ) and the driver motion are almost out of phase. All quantities exhibit sinusoidal behavior. The jet orifice velocity  $\dot{x}_{out}$  lags the cavity pressure for both the linear and the nonlinear solution. Figure 2b shows the effect of the nonlinearity of the orifice resistance. Its main effect is to shift the pressure signal such that the fluid particle velocity and the cavity pressure are almost in phase. Also, those two signals exhibit obvious nonlinear behavior due to the nonlinear orifice resistance. It is not easy however to compare these plots with the experimental data provided. Indeed, we were not clear concerning the relative phasing and data processing of the provided experimental data (piston displacement, cavity pressure, velocity measurement).

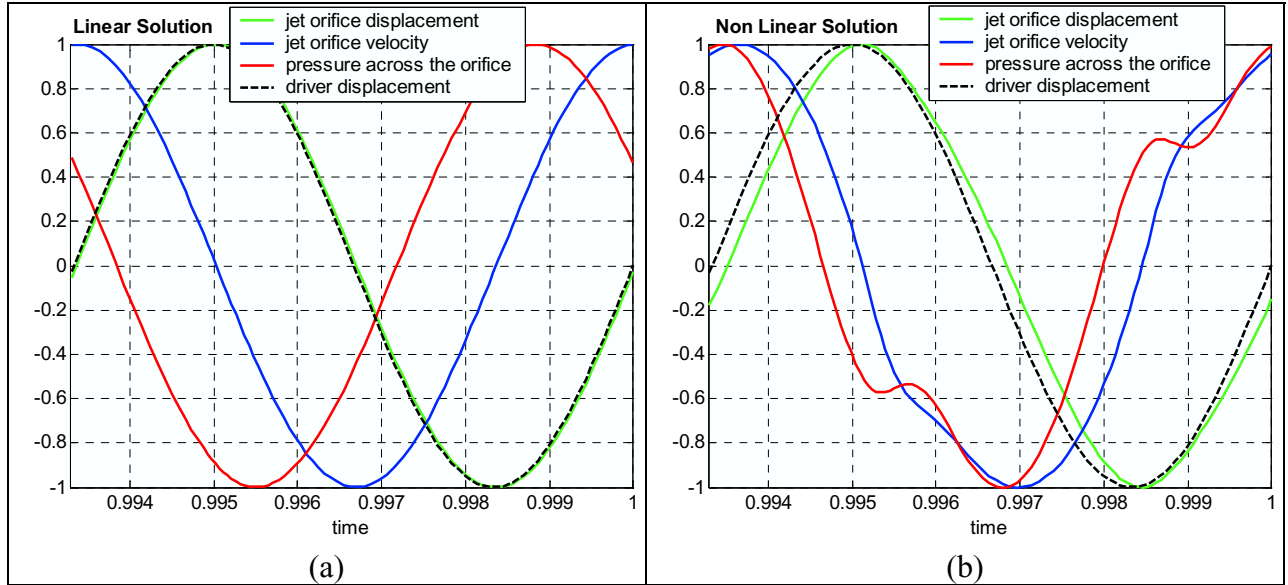


Figure 2: Time signals of the fluid particle displacement and velocity, pressure across the orifice and driver displacement during one cycle: (a) linear solution, and (b) nonlinear solution. The quantities are normalized by their respective magnitudes for comparison.

Unfortunately, our current model does not provide any information on the skewness of the velocity profile. Instead, Table 1 below summarizes a comparison between the experiments and the model output. Clearly, in its current state, the model overpredicts the output velocity and underpredicts the cavity pressure, a result that is entirely possible by overestimating the volume displacement of the driver. Given the uncertainty in this quantity, the cavity volume, and the experimental data (not reported) and the unknown effect of the small aspect ratio, beveled orifice shape (which violates the model assumptions), the discrepancy is not unexpected. We also believe that the boundary layer impedance model is not a

significant issue here since at such a low Mach number, it has little effect on the calculated device output. Experimental velocity data of the no-flow configuration ( $M_{\infty} = 0$ ) is required to address this question.

Further work is required with regards to the boundary layer impedance model to assess its validity, and it must be validated with both numerical and experimental data for a wide range of operating conditions. Such work is ongoing. In addition, we are also investigating the effect of the grazing boundary layer on the shape or skewness/distortion of the velocity profile. The results of these studies will be reported at a later date.

	$U_{CL}/U_{\infty}^{/*0}$	$\div P_{out}$ ( <i>peak-to-peak</i> ) [Pa]
Exp. (LDV)	1.31	8648
LEM	1.72 [Eq. (10)]	5115 [Eq. (11)]

Table 1: Comparison between experiments and model

<sup>/\*0</sup>  $U_{CL}$  is defined as the maximum amplitude of the phase-locked centerline velocity taken just above the orifice center.

## Acknowledgements

The authors gratefully acknowledge support from AFOSR, monitored by Dr. Tom Beutner.

## References

1. Gallas, Q., Holman, R., Nishida, T., Carroll, B., Sheplak, M., and Cattafesta, L., "Lumped Element Modeling of Piezoelectric-Driven Synthetic Jet Actuators," AIAA J., Vol. 41, No. 2, pp. 240-247, February 2003.
2. Hersh, A.S., and Walker, B., "Effect of Grazing Flow on the Acoustic Impedance of Helmholtz Resonators Consisting of Single and Clustered Orifices," NASA Contractor Report 3177, 1979.
3. Heidelberg, L. J., Rice, E. J., and Homyak, L., "Experimental Evaluation of a Spinning-Mode Acoustic Treatment Design Concept for Aircraft Inlets," NASA Technical Paper 1613, 1980.
4. Motsinger, R.E., and Kraft, R.E., "Design and Performance of Duct Acoustic Treatment," Chapter 14, Volume 2, Aeroacoustics of Flight Vehicles: Theory and Practice, NASA RP-1258, August 1991.

